Feary, D.A., Hine, A.C., Malone, M.J., et al., 2000
Proceedings of the Ocean Drilling Program, Initial Reports Volume 182

1. Leg 182 Summary: Great Australian Bight—Cenozoic Cool-Water Carbonates[1]

Shipboard Scientific Party[2]

ABSTRACT

Sediments recovered in the Great Australian Bight during Leg 182 record carbonate deposition in a middle- and high-latitude setting against the background of an evolving Southern Ocean and northward drift of the Australian continent. Approximately 3.5 km of sediment was recovered from nine sites, in water depths ranging from 202 to 3875 m. Most drilling took place on the shelf edge and upper slope, in a water depth of 202–784 m, through a mainly carbonate succession.

Two distinct groups of strata, Eocene–middle Miocene and late Pliocene–Quaternary in age, form the upper Cenozoic component of the continental margin, separated by a thin, upper middle Miocene–lower Pliocene interval characterized by slumps, sediment gravity-flow deposits, and/or unconformities. Such erosion, corrosion, and/or mass wasting and redeposition processes reflect periods of margin instability, seismicity, or lowered sea level.

The older succession consists of Eocene shallow-water terrigenous sands and carbonates that deepen upward into Oligocene and lower middle Miocene pelagic ooze and chalk. The carbonate component of this succession in shallow-water sites was poorly recovered because of irregular selective silicification. Available cored material indicates a sequence dominated by nannofossil chalk with abundant sponge spicules and characterized by stained hardgrounds and numerous omission surfaces. Downhole logs collected through all poorly recovered intervals will enable more detailed postcruise lithologic analysis for this part of the succession. In contrast, the middle Eocene–lower Oligocene succession was well recovered on the continental rise at Site 1128 in a water

[1]Examples of how to reference the whole or part of this volume.
[2]Shipboard Scientific Party addresses.

Ms 182IR-101

depth of 3875 m, and it contains an excellent expanded (>350 m) siliceous biogenic record of proto–Circum-Antarctic Current evolution.

The younger Quaternary–uppermost Pliocene package is a spectacular, extraordinarily thick (>550 m), seaward-dipping wedge of carbonate sediment on the shelf edge/uppermost slope that prograded seaward onto the Eyre Terrace and downlaps onto older sediments. Rates of accumulation exceed 40 cm/k.y., equivalent to many shallow-water tropical carbonates and twice the rate of Bahamian slope sedimentation. These green and gray carbonate strata are surprisingly uniform in composition, made up of fine carbonate sand and silt composed of skeletal fragments, mainly delicate bryozoans, ostracodes, benthic and planktonic foraminifer tests, tunicate sclerites, nannofossils, and siliceous sponge spicules. The facies transition upslope into shallower water is marked by the presence of numerous spectacular bryozoan-rich buildups. These mounds, in water depths of ~200–350 m, are characterized by numerous and diverse bryozoans, with intervening bioclastic sand and mud. These are among the first modern analogs of similar mounds that were an important component of carbonate depositional regimes in earlier Phanerozoic time.

One of the surprising discoveries of Leg 182 was the presence of a brine, varying in salinity between 80 and 105, within and underlying seven drill sites. The Cl^- distribution at three sites (Sites 1127, 1129, and 1131) suggests that the top of the brine has an essentially uniform depth below sea level and, therefore, crosscuts sequence boundaries. Although the origin of the brine has not yet been established, pore fluids in the Quaternary portion of the sediments from the shallow water sites possess a Na^+/Cl^- ratio greater than that of seawater, suggesting that fluids in these sediments had been involved in the dissolution of NaCl. As a result of high sedimentation rates and their location at the edge of a broad continental shelf, the shallow-water sites initially contained a high concentration of organic material. The brine underlying and within the Quaternary succession contains as much as three times normal seawater sulfate concentrations and, with sufficient organic material, was therefore able to produce significant amounts of hydrogen sulfide (H_2S). In addition, the relatively low iron concentration in these carbonate sediments means that the H_2S was not sequestered as iron sulfides. Consequently, H_2S concentrations were able to reach extremely high levels (>150,000 ppm). The oxidation of organic material also had an important influence on carbonate recrystallization, which is occurring at higher rates than previously thought possible for cool-water carbonates.

INTRODUCTION

Carbonate sediments and sedimentary rocks often contain a particularly sensitive record of paleoceanographic and biostratigraphic evolution. Before Leg 182, drilling on carbonate platforms had concentrated on tropical and subtropical environments. In contrast, Leg 182 investigated continental margin cool-water carbonates. These biogenic sediments, formed where seawater temperatures rarely rise above 20°C, commonly mantle continental margins in middle and high latitudes and are untapped storehouses of information regarding the evolution of global climates, eustacy, and marine biology.

The southern Australian continental margin reaches its greatest width in the Great Australian Bight (Fig. F1), making it an ideal location

F1. Leg 182 drill site locations, p. 45.

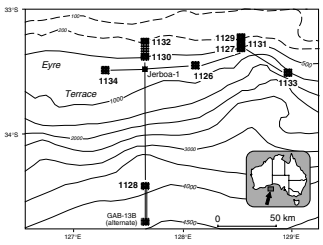

to study cool-water carbonate facies and evolution. The Great Australian Bight has been the site of cool-water carbonate sedimentation since Eocene time, resulting in an almost 1-km-thick succession, and it is now the largest area on the globe composed of such sediments. In addition, slight tectonic tilting during the late middle Miocene caused subaerial exposure of Eocene–middle Miocene strata in an extensive shallow basin. Although these sediments form a more compressed and less continuous section than the section offshore, prior to this drilling leg they provided the only basis for development of actualistic models for the formation and development of cool-water carbonates. Leg 182 drilling in the Great Australian Bight provided essential and original information to contrast the sedimentologic, paleontologic, paleoceanographic, and climatic records between warm- and cool-water realms. Postcruise analysis will also allow the development of well-constrained models that can be used in the interpretation of older Mesozoic and Paleozoic continental margin carbonate systems, as well as an isotopic and biostratigraphic record of Southern Ocean development.

Background

Tectonic Setting

The southern margin of the Australian continent is a divergent, passive continental margin that formed during the protracted period of extension and rifting that led to the separation of Australia and Antarctica in the Cretaceous and evolved during the subsequent northward drift of the Australian continent. The initial extension phase before breakup in the mid-Cretaceous (96 Ma), together with the subsequent period of slow spreading until the middle Eocene (49 Ma), resulted in deep continental margin basins filled with as much as 12 km of mainly terrigenous clastic sediments (Willcox et al., 1988; Davies et al., 1989). These basins broadly correspond to the sites of modern upper slope terraces (e.g., the Eyre Terrace at 400–1600 m depth in the western Great Australian Bight; Fig. **F1**). The onset of faster spreading in the middle Eocene also corresponded with the establishment of fully marine conditions and the initiation of carbonate sedimentation in the widening "gulf" between Australia and Antarctica. Carbonate sedimentation continued throughout the remainder of the Cenozoic as the gulf evolved first into a broad, open seaway and then into the modern Southern Ocean. Cenozoic sedimentation resulted in an extensive, relatively thin (almost 1 km thick) (Feary and James, 1998, reprinted as **Chap. 2**) Eucla Basin succession deposited in a predominantly platform-sag to platform-edge tectonic regime (Stagg et al., 1990).

Throughout the Cenozoic, the western Great Australian Bight portion of Australia's southern continental margin has been particularly stable. Interpretation of geohistory data from the Jerboa-1 exploration well indicates minimal Tertiary subsidence (Hegarty et al., 1988). Slight regional tilting (<1°?) during the late middle Miocene resulted in uplift and exposure of the Nullarbor Plain and restriction of Neogene sedimentation to the modern outer shelf and upper slope.

Cenozoic Stratigraphy of the Eucla Basin

The Eucla Basin extends inland as far as 350 km from the present coastline and seaward some 200 km to the modern shelf edge and upper slope. The Eucla Basin succession thins and feathers out inland

against Precambrian basement and gradually thickens southward to its thickest point beneath the modern shelf edge (Fig. F2). The Eucla Basin succession is entirely carbonate dominated, apart from the basal siliciclastic sequence both offshore (Sequence 7) and onshore (Hampton Sandstone), and a thin, transgressive, paleovalley-filling and strandline succession of terrigenous clastics on the inland margins of the basin.

The succession is basically divisible into two mega-sequences: a Mesozoic (Upper? Jurassic–Cenomanian; Stagg et al., 1990), siliciclastic-dominated synrift to early postrift section, and a Cenozoic (Eocene–Holocene) carbonate-dominated section. These two sections are separated by a major basinwide unconformity. The main focus of Leg 182 is the upper succession of sediments that forms an overall sigmoid-shaped series of sequences reaching a maximum thickness beneath the present-day outer shelf (Fig. F2). The stratigraphy of the lower, Mesozoic succession can be derived from the sequence intersected in the Jerboa-1 exploration well (Fig. F1); however, little information on the upper, Cenozoic section was obtained from this hole.

The extensive erosional unconformity at the top of the synrift section forms an easily recognizable and mappable surface. Seven unconformity-bounded seismic sequences have been recognized overlying this unconformity (Fig. F2) (Feary and James, 1998, reprinted as Chap. 2). One of the most striking elements of this seismic stratigraphic analysis is the identification of numerous mound-shaped structures, interpreted as biogenic mounds (Feary and James, 1995), that are present throughout the Cenozoic succession. These structures may preserve a detailed record of cool-water faunal community relationships and potentially could provide an analog for cool-water mounds recognized in the rock record, but for which no modern analogs have been identified.

The ages assigned to this succession were extremely tentative prior to drilling and are based on (1) correlation of Sequence 6B with the onshore Eucla Group (Fig. F2), (2) the similarity in depositional style between the Sequence 7 progradational wedge and Paleocene?–lower Eocene progradational sequences elsewhere along Australia's southern margin, and (3) the division of the remainder of the sequences into a reasonable time-stratigraphic framework. On this basis, the offshore sequences can be placed in the following seismic stratigraphic framework (based on Feary and James, 1998; reprinted as Chap. 2):

Sequence 7: Paleocene–middle Eocene progradational siliciclastic wedge deposited in a depositional sag, representing initial transgressive sedimentation;
Sequence 6A: middle upper Eocene to lower middle Miocene deep-water carbonates forming a multilobed sediment apron, broadly contemporaneous with Sequence 6B;
Sequence 6B: cool-water ramp carbonates with biogenic mounds (middle upper Eocene–Oligocene), passing up into an upper, warm-water, flat-topped platform rimmed by the lower? middle Miocene "Little Barrier Reef" (Feary and James, 1995);
Sequence 5: small upper middle Miocene lowstand sediment wedge with restricted distribution, lying at the foot of the steepest part of the progradational carbonate shelf escarpment zone;
Sequence 4: extensive upper Miocene aggradational deep-water carbonate ramp sequence;
Sequence 3: uppermost Miocene and lower Pliocene highstand aggradational deep-water carbonate ramp sequence;

F2. Schematic north-south diagram showing distribution and internal relationships of seven Cenozoic sequences, p. 46.

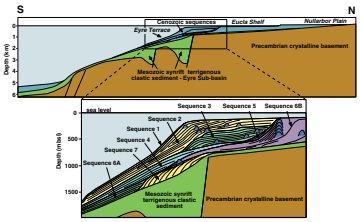

Sequence 2: thick succession of highstand Pliocene–Quaternary cool-water carbonates with spectacular clinoform ramp geometry that forms most of the modern outer shelf and contains large deep-water biogenic mounds; and
Sequence 1: thin uppermost Quaternary deep-water drape.

Existing Data

Before Leg 182 drilling, knowledge of the western Great Australian Bight margin was based on extensive high-quality seismic reflection data and a single oil exploration drill hole. Together, these provided little information about the Cenozoic succession. The original Leg 182 drilling proposals (Feary et al., 1994, 1995) were based on detailed seismic stratigraphic interpretation (Feary and James, 1998, reprinted as **Chap. 2**) of a grid of 2350 km of high-quality, regional two-dimensional (2-D) seismic reflection lines. These lines were collected and processed by the Japan National Oil Corporation (JNOC) in 1990 and 1991 over an area of 155,000 km² on the continental shelf and upper slope of the western Great Australian Bight. An additional 1380 km of moderate-quality, regional 2-D seismic lines, collected by Esso Australia in 1979 and reprocessed by JNOC, were also used to fill gaps in the JNOC dataset. The 1996 seismic site survey cruise (Feary, 1995) collected high-resolution, 80-channel generator-injector gun seismic data as 0.5-nmi-spaced grids centered on each site, together with tie-lines between sites (e.g., Fig. **F30,** p. 80, in the "Site 1126" chapter). These data permitted minor refinements of some site locations to avoid potential safety concerns.

The Jerboa-1 exploration well was drilled by Esso/Hematite in 1980 as a wildcat oil exploration well in a water depth of 761 m above a prominent tilted basement fault block located in the southern half-graben of the Eyre Sub-basin (Bein and Taylor, 1981) (Fig. **F1**). Jerboa-1 penetrated 1738 m of Cenozoic and Cretaceous sedimentary section before bottoming in Precambrian metabasalt basement, and did not encounter any significant hydrocarbon shows. The top 232 m of the hole was washed down and cased so that only 145 m of Tertiary section was actually drilled and logged. No cores were cut in this interval, so lithologic and biostratigraphic inferences are based on cuttings and downhole logs. Thermal modeling and vitrinite data (Stagg et al., 1990) indicate that the entire sedimentary section at Jerboa-1 is thermally immature (R_v = <0.65%).

SCIENTIFIC OBJECTIVES

Leg 182 was designed around six fundamental scientific topics to be addressed:

1. *The paleoceanographic history of a carbonate-dominated, midlatitude continental margin and adjacent basin during evolution of the Southern Ocean.* The Southern Ocean is one of the major controlling influences on global circulation and climate; therefore it is imperative that the oceanic history of this region be refined as much as possible. However, the paleoceanographic development of this area is not nearly as well known at present as that of the high-latitude North Atlantic (Kennett and Barron, 1992). Although there are numerous paleoceanographic problems that

can be answered by the Leg 182 drilling transect, four stand out as critical:

a. *The relationship between circulation patterns in the deep ocean and on the shelf during times of warm vs. cold ocean conditions.* The stratigraphic record in the Southern Ocean is punctuated with numerous breaks in sedimentation that are attributed to erosive periods related to increased circulation during initiation of the Circum-Antarctic Current (Miller et al., 1987; Kennett and Barker, 1990). Although such hiatuses are thought to develop on deep margins during times of lower sea level and to correlate with unconformities on the continental shelf, there are apparently continuous onshore sequences of Oligocene shelf carbonates that were deposited concurrently with erosion or nondeposition of the entire Oligocene succession on the adjacent ocean floor.
b. *The precise timing and nature of the opening of the Tasman Gateway.* Subsidence of the Tasman Rise, which permitted initiation of the cold circum-Antarctic circulation and thermal isolation of Antarctica, is one of the most important developments in Cenozoic paleoceanography (Kennett, 1982). The history of this event is poorly constrained because so much of the oceanic record is missing as a result of seafloor erosion. The Leg 182 shelf-to-basin transect is sufficiently proximal to the Tasman Rise that it should contain an excellent record of the paleoceanographic development of this seaway.
c. *The evolution and effect of the Leeuwin Current.* The first evidence for the existence of the Leeuwin Current occurred in middle Eocene time when currents from the Indian Ocean were deflected into the elongate proto-Great Australian Bight embayment. In support of this, the record of warm-water intervals is more common in the west than it is in the east, implying that the source of the water is from the west. Studies of Quaternary cores from the Great Australian Bight suggest a complex interplay between the Leeuwin Current and the West Wind Drift. This interplay appears to have had dramatic effects on primary productivity, as the Leeuwin Current is a source of warm oligotrophic waters, whereas the West Wind Drift causes upwelling of cooler eutrophic waters.
d. *The relationship between primary productivity and cool-water carbonate development.* The Leg 182 shelf-to-basin transect should contain an important record of paleoproductivity linked to upwelling. Such periods should be recorded in the biota by low species diversity, high numbers of individuals, increased sedimentation rates, and distinctive changes in stable-isotopic and trace-element compositions.

2. *The formulation of models for carbonate sedimentation on continental margins bathed predominantly by cool oceanic waters*. The deposition and accumulation of platform (neritic) carbonate sediments under cool-water (~<20°C) conditions are poorly understood compared to that of warm-water carbonates, primarily because the database is so small (Nelson, 1988; James and Kendall, 1992). Yet because of their dominantly skeletal composition, nutrient-dependent biology, and low diagenetic potential, cool-water carbonates record the history of oceanic change in ways that are profoundly different from tropical carbonates. In hydrodynamic terms, cool-water carbonate shelves are hybrids, possessing some

of the characteristics of both terrigenous clastic shelves and warm-water carbonate shelves. Sediments are produced on the shelf, in contrast to terrigenous clastic shelves where sediment is transported onto the shelf from the hinterland. Without the elevated rim that typifies warm-water carbonate shelves, however, the sediments are subject to the full sweep of oceanic waves and swells and are in this respect similar to terrigenous clastic shelves. Cenozoic exposures of inner-shelf facies in Australia suggest that storm- and wave-dominated processes tend to control deposition (e.g., Boreen and James, 1993; James and Bone, 1991). By contrast, many contemporaneous cool-water carbonate deposits in New Zealand are clearly tide dominated. Are the models of wave-dominated shelf deposition developed onshore applicable throughout the Cenozoic? All seismic profiles across the southern margin of Australia indicate that a large proportion of the youngest part of the succession is made up of prograding clinoforms (James and von der Borch, 1991; Feary and James, 1998, reprinted as **Chap. 2**). Such clinoforms seem to be signature of cool-water platforms and ramps and are postulated to be a product of accumulation dynamics (Boreen and James, 1993). There is little information regarding the composition of these deposits. Specifically, are they produced as a result of in-place, enhanced bioproduction along the shelf edge, or are they made up of finer grained material produced on the shelf and swept offshore to accumulate below the wave base?

3. *Determination of the Southern Ocean basin sea-level record, and the effect of sea-level fluctuations on stratigraphic packaging and early diagenesis of cool-water carbonates*. The Eucla margin is rich in biogenic carbonate sediments that respond in a sensitive way to variations in sea level and contain vital geochemical information needed for linking sea-level changes to paleoceanography. This information can be utilized to address two major questions of global and temporal significance.

a. *What is the detailed sea-level history of the Southern Ocean basin, and can it be linked to paleoceanographic variations?* The southern Australian neritic shelf record, derived largely from onshore successions in which the marine record is preserved only in highstand systems tracts, appears to be at odds with the global model (Haq et al., 1987) during several critical periods. Is this difference because the sediments were deposited in cool water? Through the use of a combination of physical stratigraphy and proxy paleoenvironmental parameters in a much more expanded section than exists onshore, the well-preserved Eocene–Oligocene and lower–middle Miocene successions should allow a thorough testing of this portion of the sea-level curve and resolution of specific eustatic events. The upper Miocene–Pliocene sequence is unknown onshore except for the early Pliocene highstand; so, if recovered, this will be the first clear record of this component of the sea-level record in the region.
b. *How do cool-water carbonate platforms respond to changes in sea level?* Carbonate platforms, with their chemically metastable sediments that originate largely in place, are particularly responsive to changes in seawater temperature and chemistry and variations in sea state and sea level. To date, most information on carbonate platforms has been derived from rimmed, warm-water platforms (Kendall and Schlager, 1981; Sarg, 1988). There is almost no information on the manner in which cool-water carbonate platforms respond to changes in these critical parameters

at a variety of different time scales. Specifically, we require information to describe how various segments of the shelf react during different parts of the sea-level cycle and to determine whether cold- and warm-water carbonate platforms have basically different depositional geometries as a result of the different ways the carbonate factory responds to sea-level changes.

4. *The circulation patterns of shallow subsurface fluids in an area of low hydraulic gradient and minimal recharge*. The Eucla margin is one of the few modern shelves where the onshore recharge zone is an areally vast, flat-lying karst (the Nullarbor Plain). The high primary depositional permeability of winnowed grainstones of the Eucla Shelf and the lack of early cementation suggest that significant groundwater circulation may occur, at least at shallow depths. The drive for such a circulation may be derived from the temperature contrasts between cool ocean waters and groundwaters warmed by geothermal heat flux (and possibly volcanics) within the shelf, concentrating waters on the shelf margin (Simms, 1984). Alternatively, despite inland aridity, recharge occurring over the vast continental hinterland may drive brackish to saline waters southward to discharge through the flooded shelf. Such a circulation has been recognized by James (1992), associated with cave development on the Nullarbor Plain (James et al., 1989). In contrast to the long-lived nature of the above systems, differences in sea-surface elevation on and off the shelf, associated with regional wave buildup (Feary, 1995), current flow (Rockford, 1986), and atmospheric pressure system changes, may cause pumping of marine waters into and out of the platform (Marshall, 1986).

5. *Early seafloor and shallow burial diagenesis and dolomitization of calcite-dominated sediments*. Cool-water carbonates may exhibit a radically different pattern of diagenesis compared with that of tropical aragonitic carbonates. Slow sedimentation permits seafloor lithification by intermediate Mg-calcite cements, but these appear to be volumetrically limited and localized to omission surfaces and hardgrounds that are ubiquitous in the inner platform. Indeed, both shallow-marine and meteoric cements appear to be very sparse, with magnesium being lost from high-Mg calcite (HMC) to low-Mg calcite (LMC) during grain recrystallization. Sparse calcium-rich dolomites may be present (Reeckmann, 1988; Bone et al., 1992), and at some locations replacement can be pervasive (James et al., 1993), although the fine subtidal evaporation-related dolomites typical of tropical platforms are absent. It is not known whether dolomitization is episodic, as recognized in other present-day platforms (Vahrenkamp, et al. 1991; McKenzie, et al., 1993), or occurred over extended time periods. The Eucla margin carbonates provide an opportunity to determine the present-day associations among groundwater circulation, fluid geochemistry, and diagenetic products, and, by inference from the temporal and spatial distribution of ancient diagenetic components, those that occurred under different conditions in the past. This has the potential to provide fundamental insights into the diagenesis of cool-water, open-shelf carbonates, which are direct analogs for comparable carbonate platforms that were ubiquitous during Paleozoic and other times.

6. *The pace and style of evolution of midlatitude oceanic and neritic biotas*. The Leg 182 drilling transect offered the opportunity for pioneering analysis of the Cenozoic evolution of cool-water calcareous biota, with direct applicability to studies of ancient carbonate platforms presently

lacking modern analogs. Specifically, the patterns and modes of speciation and diversification of coeval shallow- and deep-water benthic organisms as well as contemporaneous planktonic biota should be revealed. By comparing these results with those from Antarctica and the northeast Australian shelf, the geography of such processes and their relationship to physiochemical factors should be discernible.

SYNTHESIS AND RESULTS

Lithostratigraphy

Sediments recovered during Leg 182 record carbonate deposition in a mid- and high-latitude setting against the background of an evolving Southern Ocean and northward drift of the Australian continent. Sediments from the upper continental rise, in 3875 m of water at the toe of the slope (Site 1128), chronicle the change from early Paleogene time, when a humid onshore climate flushed large amounts of terrigenous clastic sediment into the deep sea, to Neogene time, when increasing continental aridity promoted mostly marine carbonate deposition. Green Eocene siliciclastic sands and silts that accumulated largely below the carbonate compensation depth (CCD) in a poorly oxygenated, bathyal setting become finer grained upward, with much of the deep-water late Eocene represented by clay deposition (Fig. F3). Initiation of the contemporary Southern Ocean circulation system, and therefore the modern global ocean, is signaled by a gradual change to lower Oligocene brown clay and carbonate, as this part of the seafloor became ventilated and the CCD deepened. The deep-water Neogene record is one of pink pelagic carbonate ooze punctuated by white planktonic foraminiferal turbidites. Late Oligocene–middle Miocene time is represented by a major hiatus and sediment gravity-flow deposits.

Most drilling took place on the upper slope and outermost shelf, in 202–784 m of water, through a mainly carbonate succession (Figs. F3, F4). Two distinct groups of strata, Eocene–late middle Miocene and late Pliocene–Quaternary in age, form the upper part of the continental margin separated by a thin upper middle Miocene–lower Pliocene interval characterized by slumps, sediment gravity-flow deposits, and/or unconformities. The older succession is stratigraphically equivalent to and roughly coeval with most of the Eucla Group, exposed onshore in the Eucla Basin beneath the Nullarbor Plain. Sediments are a package of Eocene shallow-water terrigenous sands and carbonates that deepens upward into Oligocene and lower–middle Miocene pelagic ooze and chalk (Fig. F3). Although recovery was generally poor through the Oligocene and Miocene interval because of silicification (Site 1134 is an exception for the Miocene), recovered carbonates are characterized by stained hardgrounds and numerous omission surfaces. The younger, wholly Neogene succession is a large seaward-dipping wedge of carbonate sediment that downlaps onto the older sediments and has been prograding seaward onto the Eyre Terrace since late Miocene time. The contact between the two successions is represented, particularly in the upper Miocene and especially the Pliocene, by slumps, sediment gravity-flow deposits, or unconformities. Such erosion, corrosion, and/or mass-wasting and redeposition processes reflect periods of margin instability, seismicity, or lowered sea level.

An important finding of Leg 182 was that the huge wedge of slope sediment prograding onto the Eyre Terrace is nearly entirely Quaternary

F3. Lithostratigraphic summary of the western transect, p. 47.

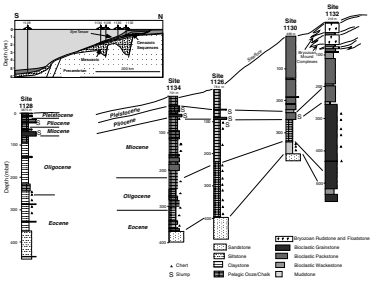

F4. Lithostratigraphic summary of the eastern transect, p. 48.

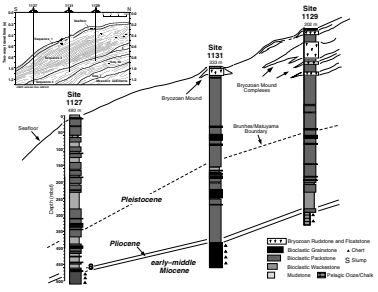

in age (Figs. F3, F4). This deposit, formed by carbonate produced on the outer shelf and upper slope and swept seaward, is more than 550 m thick in the center (Fig. F4), where rates of accumulation exceed 40 cm/k.y., equivalent to many shallow-water tropical carbonates and twice the rate of Bahamian slope sedimentation (Eberli, Swart, Malone, et al., 1997). The green and gray material is surprisingly uniform in composition, made up of fine carbonate sand and silt that was reworked in place by generations of burrowing organisms, leading to multitiered trace fossil assemblages. Particles are all skeletal fragments, mainly delicate bryozoans, ostracodes, benthic and planktonic foraminifer tests, tunicate sclerites, nannofossils, and siliceous sponge spicules. The deposit grades from mud and sand at the top, downward to partially lithified sediment in the middle, to hard limestone at the base. Sediment below 400 meters below seafloor (mbsf) is usually neomorphosed with numerous fossil molds or partially altered to sucrosic dolomite.

The facies transition upslope into shallower water is marked by the presence of numerous bryozoan-rich buildups (Figs. F3, F4). These mounds, in water depths of ~200–350 m, are dominantly muddy and characterized by the prolific growth of numerous and diverse bryozoans. The mounds in particular have seafloor relief of as much as 50 m and extend laterally many hundreds of meters. These are among the first modern analogs to similar mounds that were an important part of the carbonate depositional systems in earlier Phanerozoic time.

Biostratigraphy

Age of Sediments and Hiatuses

The Cenozoic sequence penetrated during Leg 182 mainly represents the Quaternary–Eocene. Biostratigraphic data indicate that these Cenozoic successions are mostly hiatus bound (Fig. F5), with the mid-Pliocene, lower Pliocene–upper Miocene, and upper part of the middle Miocene successions either missing or highly condensed. Other intervals of the Miocene and Oligocene are also missing, although these hiatuses are not present at all sites.

A greatly expanded Quaternary–uppermost Pliocene section was recovered at shallow-water Sites 1129, 1131, and 1127 (the "eastern transect"). The longest section at Site 1129 exceeds 555 m in thickness, with an average accumulation rate of more than 400 m/m.y. (Fig. F6). In contrast, the Quaternary–uppermost Pliocene sections only extend to ~260 mbsf at Site 1130 and ~240 mbsf at Site 1132. The Quaternary–upper Pliocene section is underlain at most sites by a thin lower Pliocene–upper Miocene interval, which in turn disconformably overlies a unit of mainly early middle Miocene age. The absence of many lower Pliocene to upper middle Miocene biozones from Sites 1129 and 1131 signifies a hiatus of at least ~7–11 m.y. This major unconformity was represented at other sites as two or three shorter hiatuses of various durations at the middle/upper Miocene, upper Miocene/lower Pliocene, and lower/upper Pliocene boundaries. They are most clearly recorded as disconformities capping the upper Miocene section at Sites 1126, 1134, and 1133 in intermediate water depths, and at shallow-water Sites 1130 and 1132 (Fig. F5). Thus, it is reasonable to speculate that the unconformity at the Quaternary–uppermost Pliocene/middle Miocene contact probably resulted from at least two major events that subsequently almost completely erased the sedimentation record of the upper middle Miocene–Pliocene.

F5. Major biostratigraphic units, unconformities, and paleobathymetric units, p. 49.

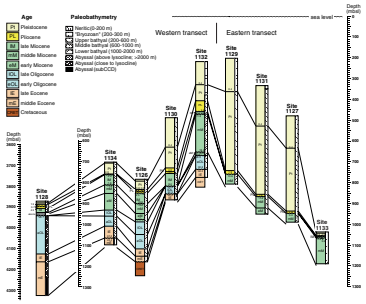

F6. Age-depth plots of biostratigraphic datum levels, p. 50.

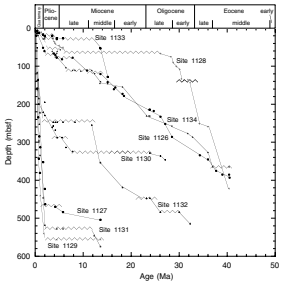

The upper Miocene succession is better represented at Site 1130 and at deep-water sites. The middle Miocene, mainly the lower part, is present at all sites except Sites 1128 and 1130, and a thin lower Miocene unit was encountered at the base of Hole 1131A (~590–610 mbsf). An expanded middle Miocene section at Site 1132 was accompanied by sedimentation rates ranging from 14 to 54 m/m.y. (Fig. F6). A similar rate of 50 m/m.y. was recorded for the middle Miocene at Site 1133. The absence of middle–lower Miocene biofacies from Sites 1130 and 1128 is interesting because these two sites respectively represent intermediate and deepest water sites along the depth transect. At Site 1130 (488 meters below sea level [mbsl]), the upper Miocene section is disconformably underlain by sediments of mainly early–middle Oligocene age, indicating a depositional gap of ~15 m.y. At Site 1128 (3875 mbsl), the entire middle Miocene–upper Oligocene interval corresponds to a ~15-m-thick debrite with mixed calcareous nannofossil and planktonic foraminiferal assemblages of early–late Miocene age, suggesting an unconformity totaling ~13 m.y. in duration. Sites 1126 and 1134, two intermediate-water sites, exhibit generally similar assemblage compositions, ages of recovered sediments, and position and number of hiatuses. These are the only sites yielding definite lower Miocene calcareous nannofossils and planktonic and benthic foraminifers.

Sediments of Oligocene age and older were recovered at Sites 1126, 1128, 1130, 1132, and 1134 (the "western transect"). At Sites 1130 and 1132, the Oligocene section probably overlies Eocene sediments disconformably, and a hiatus of ~2 m.y. is indicated by biostratigraphic data. However, the zonal succession of nannofossils and planktonic foraminifers is largely continuous across the Oligocene/Eocene boundary, suggesting a conformable succession at Sites 1126, 1128, and 1134. Mainly lower Oligocene assemblages are present at Sites 1128, 1130, and 1132 in the west, and an expanded lower Oligocene section is indicated by nannofossils at Site 1128. Biostratigraphic resolution below 70 mbsf at Site 1128 was largely achieved by calcareous nannofossils because planktonic foraminifers were rare or barren in sediments dominated by siliceous oozes and packstones.

Holes 1126D and 1134A are the only holes containing rich calcareous microfossils of Eocene age. Poor preservation, however, impaired proper recognition of species and biozones in some intervals. Although present at all western sites, the middle Eocene is represented by poorly preserved, impoverished assemblages in various poorly recovered lithologies. The Eocene is represented by a siltstone (~150 m thick) with sporadic nannofossils at Site 1128; a calcareous packstone (~30 m thick) with moderately preserved nannofossils and planktonic and benthic foraminifers at Site 1126; and a dark, iron-stained sand (30 m thick) with rare and poorly preserved microfossil assemblages at Site 1134. A calcareous sandstone at Site 1130 and a bioclastic limestone at Site 1132 both contain shallow-water associations of planktonic and benthic foraminifers. No calcareous nannofossils or foraminifers were discovered in the dark green sandstone at the base of Hole 1126D, which may correspond to Cretaceous synrift sediments along the southern Australian margin.

Paleobathymetry and Paleoceanography

The succession of microfossil assemblages from Leg 182 provides an excellent record of Eocene–Holocene sea-level and circulation changes in the Great Australian Bight. Expanded Quaternary successions at Sites

1127, 1129, 1130, 1131, and 1132 contain upper bathyal benthic foraminiferal assemblages with a redeposited neritic component. Apparent fluctuations in the relative proportions of neritic taxa and upper bathyal taxa indicate that downslope transport periodically varied in intensity during the Quaternary. These changes, together with the periodic intrusion of warm-water species into temperate planktonic foraminiferal assemblages, indicate responses to changing climate and oceanic circulation. Calcareous nannofossil assemblages dominated by *Braarudosphaera bigelowii* indicate that a major ecological crisis affected the planktonic ecosystem near the base of the Quaternary–uppermost Pliocene.

At three shallow-water sites (Sites 1129, 1131, and 1132), diversified, extremely well preserved benthic foraminiferal assemblages, including unusually large specimens (>1 mm), are found together with abundant and well-preserved bryozoan fragments (Fig. F5). These assemblages were probably part of a highly dynamic ecosystem that became established at the seafloor during the Quaternary, coincident with bryozoan buildups in paleodepths of 200–300 m. A shallowing-upward trend from middle bathyal paleodepths in the middle and late Miocene to upper bathyal paleodepths in the Quaternary is recorded at Sites 1129, 1130, and 1132 (Fig. F5). Middle bathyal faunas at these sites reflect middle and late Miocene transgressive pulses that are also expressed onshore in southern Australia by thin transgressive tracts.

Middle bathyal assemblages from upper Eocene–upper Miocene successions show major changes in composition at intermediate-water Sites 1126 and 1134. The most severe changes in the early Miocene probably relate to global changes in deep- and intermediate-water circulation affecting the distribution of bathyal benthic foraminifers worldwide. The composition of abyssal assemblages at Site 1128 indicates deposition above the CCD during the Quaternary–latest Pliocene, close to the lysocline in the late Oligocene–middle Eocene, and below the CCD in the early–middle Eocene in the deep basin (Fig. F5). Assemblage boundaries appear to be coeval in the Eocene, Oligocene, and lower Miocene of intermediate- and deep-water Sites 1126, 1128, and 1134, suggesting that benthic foraminifer distribution was controlled by major environmental changes during these periods. Discrepancies between assemblage boundaries of deep-, intermediate-, and shallow-water sites in the middle Miocene–Quaternary sequence relate to stratigraphic or lithologic differences and reflect distinct depositional and paleoceanographic regimes in the region.

Paleomagnetism

Previous carbonate legs have proved very unsatisfactory for paleomagnetists because the magnetic intensity of the sediments was so low that remanence measurements were essentially unreliable. However, with the change to direct-current superconducting quantum interference devices in the new instrument, it was possible to measure the magnetization at most sites during Leg 182. Nevertheless, the natural remanent magnetization (NRM) of sediments from Sites 1126 and 1134 was so weak that, after a coring overprint was removed, the magnetization of much of the sediment was at the noise level of the instrument.

Coring Experiments

During Leg 182, an experimental nonmagnetic cutting shoe was used in advanced hydraulic piston corer (APC) coring (see **"Appendix: Magnetics Experiment"**). The shoe and other components of the bottomhole assembly were used to investigate anomalous magnetization observed in cores. Comparisons were made between cores taken with (1) standard core-barrel assemblies, (2) standard core-barrel assemblies and the nonmagnetic shoe, and (3) nonmagnetic core barrels and shoe. On some occasions, it was clear that the nonmagnetic shoe and assembly greatly improved the paleomagnetic record. On other occasions, the shoe alone improved the record compared with the standard core-barrel assemblies. However, there were also sites where neither the nonmagnetic shoe nor the entire nonmagnetic core-barrel assembly had any obvious effect. This is consistent with the intermittent nature of the anomalous magnetization experienced during past legs. Postcruise work will focus on trying to isolate other sediment properties such as grain size, porosity, or shear strength, which may control the distribution of coring contamination.

Rock Magnetism

A common feature of the rock magnetism in the upper sections of Leg 182 holes was the extremely high ratio of anhysteretic remanent magnetization to isothermal remanent magnetization (ARM/IRM). This is a measure of the degree to which single-domain particles dominate among the magnetic phases present in the samples. This ratio generally decreased downhole and was accompanied by a decrease in intensity of magnetization and coercivity. This decrease in magnetization intensity is generally interpreted as dissolution of the finest grained magnetic phases in the sediment. IRM acquisition suggests that magnetite and magnetic sulfides are the principal remanence carriers. The observation of a downhole decrease in ARM/IRM and intensity is consistent with diagenetic models involving organic matter oxidation and sulfate reduction as the principal processes that regulate the preservation of ferromagnetic phases.

Magnetostratigraphy

Long-core and discrete sample measurements yielded a record of inclination from which a Pliocene–Quaternary magnetostratigraphy was interpreted. Overall, deeper water records are of good to fair quality, yielding accurate estimates of the expected inclination for the present latitude. In contrast, lower intensities in the shallow-water sites result in shallow inclinations with large scatter. The Brunhes/Matuyama boundary was identified in five high-sedimentation-rate sites (Fig. **F7;** Table **T1**). The Jaramillo Subchron (C1r1n) and the top of the Olduvai Chron (C2n) were also found at three sites. The interpretation of magnetic polarity in Figure **F7** implies that sedimentation rates in the early Quaternary–latest Pliocene were considerably lower than during the Brunhes Chron. In addition, variations in the intensity of the remanence after partial demagnetization were found to oscillate on time scales comparable with those of the geocentric axial dipole. Although the intensities have not been normalized to account for variations in concentration, these sediments may provide a valuable relative paleointensity record that can be used for high-precision correlation between

F7. Summary of paleomagnetic data and magnetostratigraphy, **p. 51.**

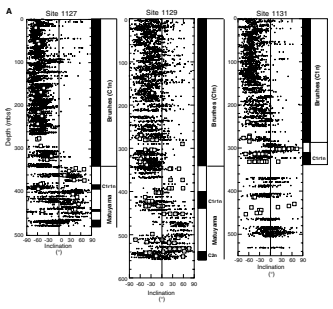

T1. Summary of Quaternary magnetostratigraphy, **p. 57.**

sites. For Sites 1126 and 1134, magnetostratigraphic data were obtained for parts of the Miocene. Site 1128 also contains a long record of the early Oligocene polarity sequence.

Geochemistry

The drilling of nine sites off the Eucla margin provided a unique insight into the fluid dynamics along a continental margin dominated by cool-water carbonates. The most significant discovery was the presence of a brine, varying in salinity between 80 and 105, that was present in and underlying seven of the nine sites (the exceptions being Site 1128, drilled in a water depth of 3884 m, and Site 1133). At Site 1133 (located in 1043 m of water) fluids were encountered with a salinity of 40, but recovery problems precluded the measurement of the salinities in deeper samples. The brine was present at relatively shallow depths at the deeper sites (1134 and 1126), whereas maximum salinities were not encountered until depths ≥400 mbsf at the shallower sites (Sites 1127, 1129, 1130, 1131, and 1132). The impact of the brine is more readily apparent along the eastern transect (Sites 1127, 1129, and 1131; see Fig. F4). Similar processes appear to occur at Sites 1130 and 1132, although they are reduced in nature.

At Sites 1127, 1129, and 1131, a gradual increase in salinity was encountered, reaching a maximum value of ~100 at Site 1127 (farthest seaward) and 92 at Site 1129 (closest to the shelf). Pore fluids in these Quaternary portion of the sediments from these sites also possess a Na^+/Cl^- ratio exceeding that of seawater, suggesting that the fluids in the sediments had been involved in the dissolution of NaCl. Although the origin of the fluids has not yet been established, a probable explanation is that they formed during the Quaternary when the Eucla shelf was exposed numerous times during sea-level lowstands. We suggest that large hypersaline lagoons developed during these episodes of low sea level. Because of the greater hydrostatic head, fluids with high salinity were forced into underlying strata and out onto the adjacent continental slope. During sea-level highstands, high-salinity fluids then diffused upward as additional sediment was deposited, and the profiles of individual ions were modified by diagenetic reactions in the sediments. This sequence of events probably occurred a number of times as sea level fluctuated during the Quaternary. This hypothesis is supported by an examination of the Cl^- distribution at the three sites (Fig. F8), which suggests that the top of the brine has a common depth below sea level and, therefore, crosscuts sequence boundaries.

All three sites exhibited high concentrations of H_2S and methane, combined with high values of alkalinity. The high concentrations of H_2S are derived from the oxidation of organic material by sulfate-reducing bacteria. The relatively low concentrations of iron in carbonates, in contrast to siliciclastic-rich environments, means that the H_2S is not sequestered as iron sulfides. Consequently, concentrations of H_2S are able to reach high levels (>150,000 ppm at Site 1131). As a result of the high rate of sedimentation (>200 m/m.y.) and the position of the sites close to the continental shelf, these sites contained an initially high concentration of organic material. Under normal conditions, organic material would be oxidized first by oxygen and then by sulfate-utilizing bacteria, thereby creating alkalinity and H_2S. Although this process also takes place on the Eucla margin, the high-salinity brines underlying and within the Quaternary succession provide as much as three times the

F8. Contour plot of Cl^- concentration at Sites 1127, 1131, and 1129, p. 53.

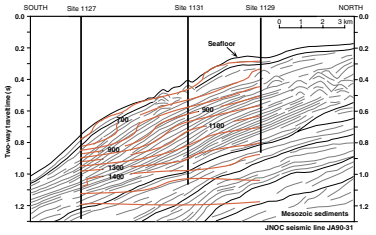

normal seawater sulfate concentrations; therefore, with sufficient organic material, significantly higher amounts of H_2S can be formed. As the sediments are buried, the concentration of sulfate is depleted in the sediment and a gradient is established between the sediments, the overlying seawater, and the underlying brine. As a result of the high sulfate concentration of the brine, the flux of sulfate diffusing into the zone of organic material remineralization is significantly greater than in a normal marine sediment, resulting in greater than normal sulfate reduction and higher alkalinity.

In addition to H_2S, high concentrations of methane and the presence of other higher molecular-weight hydrocarbons were discovered in the sediments at Sites 1127, 1129, and 1131. At Site 1127, gas pockets in the core were found to contain as much as 73% methane and 365 ppm ethane. We suggest that these gases, including the higher molecular-weight hydrocarbons, are bacterial in origin and generated in situ. Higher molecular-weight alkanes are generally only believed to form through thermogenic processes. However, the concentrations of ethane, propane, and butane did not increase with depth, but instead reached a maximum associated with the maximum in methane, indicating that these gases also originated within this portion of the sediment and were not thermogenic in origin (Fig. **F9**).

The oxidation of organic material also has an important influence on carbonate recrystallization. The sediments at all sites cored during Leg 182 initially contained a mixture of aragonite, HMC, and LMC. Of these minerals, aragonite and HMC are metastable and alter to the more stable LMC and dolomite. This process is evident at all sites drilled, and is greatly accelerated by the processes of sulfate reduction and consequent formation of H_2S. During the oxidation of organic material, two important chemical reactions take place that alter the carbonate chemistry in the pore waters: (1) sulfate reduction creates two moles of alkalinity for every mole of sulfate that is consumed, and (2) one mole of H_2S is produced ($2CH_2O + SO_4^{2-} = H_2S + 2HCO_3^-$). The H_2S dissociates in pore water, causing the pH to be reduced and the speciation of carbonate in the pore waters to move from being dominated by HCO_3^- to H_2CO_3. This sequence of events produces pore fluids that are undersaturated with respect to the metastable carbonate minerals. The most thermodynamically soluble form of calcium carbonate, HMC, dissolves first, followed by aragonite and then LMC. This trend is observed at all sites. The high-alkalinity environment creates a thermodynamic regime favorable for the formation of dolomite. Dolomitization consumes Mg^{2+} from pore waters, setting up a strong diffusive gradient into the reaction zone from the overlying seawater and underlying brine. The formation of dolomite at Sites 1127, 1129, and 1131 is well illustrated in Figure **F10,** which shows concentrations of ~5% at Sites 1127 and 20% at Sites 1129 and 1131.

Although the high-salinity pore fluids were also present at most other sites (Sites 1130, 1132, 1126, and 1134), these sites showed lower concentrations of H_2S and methane and consequently lower amounts of carbonate diagenesis. The controlling factor at these sites is the supply of organic material combined with the sedimentation rate.

F9. Concentration of gases in headspace samples, Site 1129, **p. 54.**

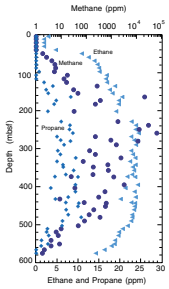

F10. Concentration of dolomite, Sites 1127, 1131, and 1129, **p. 55.**

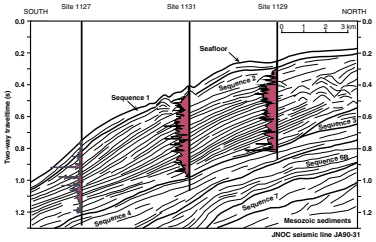

Petrophysical and Downhole Measurement Data

Downhole logging data were collected at eight of nine sites drilled during Leg 182. To complement these data, an extensive program of

sediment physical properties measurements was undertaken. The presence of chert, particularly in the pre-Quaternary sedimentary sequences, resulted in low recovery. Analysis of downhole logging data will provide the information necessary to fill in recovery gaps, refine the placement of lithostratigraphic boundaries, and enable interpretation of sedimentary facies, composition, and structure within missing intervals. Check-shot surveys conducted at five sites will facilitate correlation of the drilled strata to the regional grid of high-resolution seismic data.

The downhole logging and physical properties measurement program undertaken during Leg 182 provided the opportunity to investigate early and postdepositional diagenesis in a nontropical carbonate system. A significant result of Leg 182 was the determination that nontropical carbonates display diagenetically driven mineralogical, geochemical, and textural changes that are similar to those occurring in tropical carbonates, which is contrary to the notion that cool-water carbonates have relatively low diagenetic potential because of their dominantly LMC mineralogy. Nevertheless, our analyses indicated that sediment alteration and cementation were not as extensive as seen in warm-water carbonates. In tropical carbonates, diagenesis results in distinctive, widely ranging physical properties measurements: *P*-wave velocity (~1.5–6 km/s), porosity (~10%–80%), and bulk density (~1.5–2.8 g/cm^3) (Eberli, Swart, Malone, et al., 1997). Petrophysical investigations during Leg 182 show that equivalent variations within cool-water carbonate sediments are much less dramatic: *P*-wave velocity (~1.5–2.2 km/s), porosity (~30%–60%), and bulk density (~1.5–2.0 g/cm^3).

An important finding of Leg 182 was the discovery of distinct, possibly Milankovitch cyclicity recorded in gamma-ray and density data from the thick Quaternary sediment wedge drilled at numerous upper slope/shelf edge sites (e.g., Fig. **F11**). The high sedimentation rates within this sequence, in excess of 40 cm/k.y., will enable high-resolution frequency analysis of the logging and physical properties datasets that will assist in the refinement of the biostratigraphic ages within this time interval. Formation MicroScanner (FMS) data collected at six of the logged holes will permit detailed investigation of depositional facies and sedimentary structure within the sediment cycles, particularly in those intervals where recovery was poor. Correlation of the cyclicity present in the temperate-water carbonate wedge to that in other Quaternary carbonate and noncarbonate continental margin systems will provide important information on differences in eustatically influenced sedimentation patterns.

F11. JNOC seismic Line JA90-31 for the eastern drilling transect, overlain with spectral gamma radiation, bulk density, and porosity from downhole logs, **p. 56.**

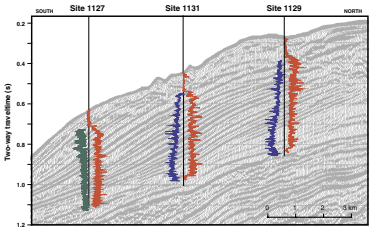

PRINCIPAL RESULTS

Site 1126

Site 1126 is located on the eastern Eyre Terrace upper slope in 783.8 m of water. This site was designed to intersect Cenozoic seismic Sequences 2, 3, and 4, and Lobes 1 and 3 of Sequence 6A and to intersect as much of the upper part of the Cretaceous section as time permitted. The target depth at this site was a high-amplitude reflector of probable Cenomanian age, estimated before drilling (on the basis of stacking velocities) to be at 525 mbsf. Because this was also the first Ocean Drilling Program (ODP) site in this basin, it provided the opportunity to estab-

lish a basic stratigraphy for the Cenozoic sequences that could then be refined at later sites.

Five lithostratigraphic units were delineated at Site 1126. Unit I (0–60.2 mbsf) is a calcareous ooze with a gradational alternation between two major sediment types: (1) white-gray nannofossil-rich matrix-supported ooze and (2) light gray grain-supported ooze rich in planktonic foraminifers. Unit II (60.2–116.8 mbsf) is characterized by several intervals of slumped calcareous ooze. Sediment composition in these bodies is the same as in the undisturbed sediments. The first downhole occurrence of silicified layers (porcellanite) subdivides Unit II into an upper Subunit IIA and a lower Subunit IIB. As in Unit I, intervals that are not affected by slumping display a light/dark alternation. In the lower part of Unit II, these cycles are increasingly asymmetric, with the dark portions becoming dominant. Unit III (116.8–166.5 mbsf) consists of calcareous ooze with interbeds of silicified layers in the upper part of the unit. The lower part of the unit is porcellanite free and displays the same type of cyclicity as sediments in the overlying units. Unit IV (166.5–396.6 mbsf) coincides with an interval of low core recovery and thus cannot be described in detail. It consists of an alternation of calcareous ooze to chalk intervals and silicified pelagic limestones with some planktonic foraminifers and bioclasts. Unit V (396.6–455.9 mbsf) consists of black to green sandstones, silty sandstones, clayey siltstones, and minor granule conglomerates.

Nannofossil and planktonic foraminifer biostratigraphies show that Quaternary–middle Eocene sequences were recovered. Sandstones of probable Cenomanian age (Unit V) recovered at the base of the drilled interval are barren of marine microfossils. Sedimentation rates were relatively high in the Quaternary–uppermost Pliocene (31 m/m.y.) and lower Pliocene (24 m/m.y.) and slow in the remainder of the Neogene and Paleogene sections, where rates alternate between 7–8 m/m.y. and 11–15 m/m.y., with faster rates in the upper Miocene, lower Miocene, and upper Oligocene. At least two disconformities or condensed intervals are present at the Miocene/Pliocene and lower/middle Miocene boundaries. Benthic foraminiferal assemblages show a change in benthic environments from lower bathyal to middle bathyal in the upper part of the middle Eocene nannofossil zone (NP16). Slumps between ~55 and 110 mbsf are marked by a mixture of upper Miocene and lower Pliocene planktonic taxa found within an uppermost lower Pliocene assemblage. The slump is also flagged by a mixture of a displaced upper bathyal assemblage of benthic foraminifers found within an in situ middle bathyal assemblage.

The results of paleomagnetic long-core measurements of cores from Hole 1126B and 1126C were disappointing. The NRM was dominated by a vertically downward coring contamination that was largely removed by 20 mT demagnetization, whereupon the signal was almost uniformly reduced to the noise level of the instrument. In addition, there were anomalous peaks in intensity near the tops of most cores and of several sections. These were so large that we interpret them as contamination. Only a single core gave a sequence of reversals that could be interpreted magnetostratigraphically. A comparison between whole-core and archive-half core measurements showed that the two measurements of inclination are not significantly different, but there are systematic differences in declination. The nannofossil chalks gave stronger signals, but poor recovery precluded determination of a useful magnetostratigraphy. In the sandstone recovered toward the base of Hole 1126D (Unit V), normal magnetizations were observed. Their high

inclination, giving a paleolatitude of ~50°S, is in accordance with northerly motion of the Australian plate as it moved away from the Antarctic-Australia spreading center. Rock magnetic properties of representative samples from the various sedimentary units differ in a manner that is consistent with the NRM variation. In the nannofossil chalk and in some of the more strongly magnetized nannofossil oozes, the magnetic carrier appears to be single-domain magnetite consistent with a magnetotactic bacterial origin, whereas a different and harder phase dominates in the uppermost nannofossil ooze sediments.

The upper 154.0 m of sediment at Site 1126 was double cored. Construction of the composite section from Holes 1126B and 1126C indicates that a complete record of the sedimentary section was not recovered. Correlation between cores was hindered by significant differential core distortion, particularly at the very top of each core where an expanded record was indicated. Correlations were further hindered by a decrease in core recovery below 100 mbsf, resulting from the presence of multiple chert layers. Below 60 meters composite depth (mcd), large data gaps and the presence of numerous slumps made correlations difficult and highly tentative. The composite section indicates gaps in the record at ~26–27, 64–65, 73–74, 86–87, 109–112, 124–125, and 130–137 mcd.

Only low concentrations of methane and ethane were detected at Site 1126. Methane ranges from 2.2 to 13.6 ppm. Ethane is present in five samples between 186.5 and 236 mbsf (1.1–2.7 ppm) but is not detected at greater depths. The carbonate content is uniformly high (80–91.2 wt%) in the upper 116 mbsf but becomes highly variable (30.6–93.2 wt%) from 116 to 254.2 mbsf. Because of poor core recovery, no samples are available in the interval from 254.2 to 348.6 mbsf. From 348.6 to 389.6 mbsf, the carbonate content returns to high levels within a narrow range (79.5–90.0 wt%), dropping again to very low values in sandstones (0.4–0.6 wt%) from 406.4 to 454.5 mbsf. Total organic carbon is low throughout the cored interval except for the bottommost sample of Hole 1126D, which has 1.33 wt% organic carbon. All other organic carbon values are less than 0.8 wt% and most are less than 0.2 wt%

Site 1126 is characterized by a large increase in salinity that manifests itself as shallowly as 10 mbsf, reaching a maximum of 106 (about three times normal seawater salinity) by a depth of ~100 mbsf. Most of the other geochemical parameters exhibit nonconservative behavior with respect to Cl^-, including Ca^{2+} which shows a net excess, and Mg^+, SO_4^{2-}, and alkalinity, all of which show net losses. The pore waters have a Na^+/Cl^- ratio close to that of seawater.

Physical properties data closely reflect the location of sequence boundaries and changes in lithology and mineralogy. These data were divided into five units on the basis of shifts in measured parameters. Physical properties Unit (PP Unit) 1 is characterized by high natural gamma radiation (NGR) with a trend of increasing *P*-wave velocity and bulk-density measurements to the bottom of the unit. The base of PP Unit 1 broadly coincides with the upper Pliocene/Pleistocene boundary. Physical properties Unit 2 is characterized by relatively high NGR that dramatically decreases toward the base of the unit. This decrease occurs because of the downhole disappearance of aragonite. *P*-wave velocity increases throughout PP Unit 2, as does thermal conductivity. The base of the unit coincides with the upper Pliocene/lower Miocene boundary. Physical properties Unit 3 is characterized by low variability in *P*-wave velocity and NGR. The base of this unit was not recovered in the sedi-

ments, but can be defined at 185 mbsf using downhole logs. Physical properties Unit 4 is characterized by alternations of high-velocity porcellanite and lower velocity oozes. This high contrast in sediment induration was probably the major cause of the low recovery in this unit. The top of PP Unit 5 coincides with a major hiatus at the base of the Tertiary. Physical properties Unit 5 shows much greater NGR values and higher *P*-wave velocities, reflecting the transition from PP Unit 4 ooze into PP Unit 5 sandstone. This indicates that PP Unit 5 sediments were affected by diagenesis. Thermal conductivity co-varies with water content, bulk density, and *P*-wave velocity.

Hole 1126D was logged with three tool strings: the triple combination logging tool (triple combo), sonic/geologic high-resolution magnetic tool (GHMT) combination, and the well seismic tool (WST). The FMS tool was not run with the sonic tool as usual because of (1) excessive heave caused by dual swell directions, which was not compensated for by the wireline heave compensator, and (2) a large hole diameter, as indicated by the caliper on the triple combo. The WST was used for recording nine check-shot stations between 420 and 130 mbsf. Several washed-out zones affected readings made by excentric tools (e.g., neutron porosity and density), whereas readings measured by hole-centered tools (e.g., magnetic susceptibility [MS], sonic, and resistivity logs) were little influenced by hole conditions. The MS data were useful for subdividing the measured section into 10 provisional logging units, some of which correlate with the seismic stratigraphic units. In the interval below 160 mbsf where core recovery was poor, changes in several logs provide the detail and continuity necessary to further subdivide the section. The spectral gamma-ray log measured by the triple combo proved very useful for correlating the part of the section measured through pipe (upper 116 mbsf) with core measurements. In the lower siliciclastic part of the section, photoelectric effect (PEF) values indicate the presence of iron minerals.

The check-shot survey showed that the actual time–depth conversion curve fell within the narrow envelope of time–depth curves derived from stacking velocities, so depth estimates for other sites based on stacking velocity curves can be viewed with more confidence. The preliminary biostratigraphic data permitted ages of the regional Cenozoic seismic sequences to be defined, showing that Sequence 2 corresponds to the Pleistocene–latest Pliocene, Sequence 3 is of middle–late Miocene age, Sequence 4 is of early Miocene age, and Sequence 6A is of Eocene–Oligocene age.

Site 1127

Site 1127 was the first and most seaward site of a three-site transect through a spectacular set of upper Neogene clinoforms immediately seaward of the present-day shelf edge. Site 1127, located on the upper slope in 479.3 m of water, intersected an expanded record of the youngest clinoforms as well as the lowest, more condensed portion of the clinoform sequence. The principal objective of this transect was to collect detailed high-resolution profiles through a late Neogene shelf edge (high energy) to upper slope (low energy) succession deposited within a cool-water carbonate environment to determine the response of this type of depositional system to Pliocene–Quaternary sea-level fluctuations.

At Site 1127, we recovered a 510.7-m-thick (Table T2) monotonous succession that is dominated by very fine to fine-grained, heavily bio-

T2. Summary of operations, p. 58.

turbated, unlithified to partially lithified, greenish gray wackestones to packstones, made up of three units. Unit I (0–6.0 mbsf) consists of two subunits: an upper nannofossil ooze and a lower foraminiferal ooze. Unit II (6.0–464.5 mbsf) consists of alternating bioclastic wackestone- and packstone-dominated packages with thin grainstone beds divisible into five subunits. These subunits are characterized by a lower portion composed of wackestones to packstones, grading up into wackestones, and dominated at the top by packstones with thin capping grainstones. Shallower water fauna are most abundant near the top of each subunit. The lowermost subunit (~420–464.5 mbsf) has a slumped base with abundant clasts, including bryozoan and large skeletal fragments within an ooze matrix. Unit III (464.5–510.7 mbsf) consists of an upper nannofossil ooze and a lower glauconite-rich bioclastic packstone, with minor capping grainstone beds with intraclasts.

Calcareous nannofossils and planktonic foraminifers indicate an extraordinarily expanded Quaternary–uppermost Pliocene sequence of ~470 m, with a hiatus of ~3 m.y. between basal Quaternary–uppermost Pliocene (Zone NN19) and underlying Miocene sediments. Based on preliminary biostratigraphic datum levels, average sedimentation rates were 240 m/m.y. in the Quaternary and 2–8 m/m.y. in the Miocene. The thin Miocene section contains a strongly mixed planktonic foraminiferal assemblage. A well-preserved benthic Pleistocene foraminiferal assemblage is recognized down to 414.5 m. Between 414.5 and 501.1 mbsf, we identified two benthic assemblages that contain mainly upper bathyal taxa but include large numbers of abraded and corroded tests, indicating extensive mixing or reworking. Quaternary benthic foraminiferal assemblages often display a uniformity in test size and lack of medium to large tests that is consistent with grain-size sorting and downslope redeposition. The cool temperate Quaternary fauna is accompanied by warm-water species at various intervals, probably reflecting a combination of global climatic fluctuations and regional paleoceanographic variations, especially in relation to the flow of the Leeuwin Current.

Paleomagnetic measurements revealed a long section of normal polarity to 343.4 mbsf, which we interpret as the Brunhes Chron. The mean inclination was –49.9° with a standard deviation of 22°. It was only possible to locate a very approximate onset (380 mbsf) and end (395 mbsf) of the Jaramillo Subchron. We found intensity fluctuations within the Brunhes Chron in the NRM after 20 mT demagnetization that appear to correlate with standard records of geomagnetic field fluctuations back to 400,000 yr. The calculated sedimentation rate for the whole Brunhes Chron is 480 m/m.y., whereas the rate for the first 400,000 yr based upon the intensity estimation is 277 m/m.y. Rock magnetism analysis revealed that the dominant magnetic phase was chemically unstable, so that the saturation remanence decayed by as much as 60% within 48 hr. This behavior is typical of the ferromagnetic sulfide greigite, which inverts sluggishly to paramagnetic pyrite. The high ARM/IRM suggests a dominant single-domain grain size and a strong magnetotactic bacteria input. However, if this suggestion is correct, the magnetotactic bacteria synthesize greigite rather than magnetite.

The most striking organic geochemical results at Site 1127 are the very high concentrations of methane and H_2S present throughout the section. Gas pockets within the core were common from 47 to 312 mbsf, and these were sampled directly through the core liner with a gas-tight syringe (vacutainer). Methane concentrations in these gas pockets

range from 329,000 to 585,000 ppm. Hydrogen sulfide ranges from ~60,000 to 138,000 ppm. Methane is present at lower and highly variable concentrations in headspace samples, with the lowest values at the top and bottom of the drilled interval. Methane/ethane ratios in vacutainer samples decrease downhole from 2728 to 1309, with a decrease in the ratio to 174 in headspace samples. Carbonate content values predominantly range between 85 and 92 wt%, with a trend toward lower values with increasing depth. Organic carbon values are primarily in the range of 0.1–0.6 wt% down to ~250 mbsf and then vary from 0.5 to 1.0 wt% to the bottom of the hole.

Although similarly influenced by high-salinity pore fluids (as much as 100 in Pliocene and older portions of the section), pore-water geochemistry at Site 1127 was fundamentally different than at Site 1126 because of an extended sulfate reduction zone. As a result of the more inshore location, Site 1127 not only had a higher initial organic matter content compared to Site 1126, but more of the organic material was preserved as a result of higher sedimentation rates. As a result of the high sulfate concentration in the deeper, higher salinity fluids, the sulfate reduction zone is enlarged and the consequent production of H_2S is much higher than in normal organic-rich sediments. In addition, the relatively iron-poor nature of these sediments precludes the formation of iron sulfide phases that would normally sequester H_2S. The greatest amount of carbonate recrystallization appears to occur at the lower interface between the sulfate-depleted zone (~180 mbsf) and the underlying sediments, where sulfate is actively diffusing upward from the higher salinity fluids below. This process produces pore fluids undersaturated with respect to metastable carbonate minerals, causing the precipitation of LMC and dolomite. Striking variations in the amount of LMC, HMC, aragonite, and dolomite also occur throughout the succession, with presumed sea-level lowstands characterized by increased HMC and the presence of dolomite.

As a result of disruption of the sediments during degassing, laboratory physical properties measurements are of limited value for developing a downhole stratigraphy. However, the NGR measurements were only affected to a minor extent and can be used to define three PP units. Physical properties Unit 1, from 0 to 130 mbsf, is characterized by three high-amplitude cycles superimposed on a rising trend. Physical properties Unit 2 occurs from 130 mbsf to the base of the uppermost Pliocene–Quaternary unit at 467 mbsf, which is marked by a sudden decrease in NGR values. This unit is characterized by low-amplitude, high-frequency cyclicity in NGR values. Physical properties Unit 3 corresponds to the lower Pliocene sediments below the seismic Sequence 2 boundary, which are also significantly denser than the Quaternary sediments.

Hole conditions were excellent for logging, with most caliper readings within 10 cm of bit size. Hole 1127B was logged with three tool strings: the triple combo and FMS/sonic to the mudline, and the GHMT to 59 mbsf. The triple combo was run without the nuclear source in the hostile environment lithodensity sonde because of safety concerns; consequently, density logs are not available for this site. During and after logging, close examination showed that there was no obvious damage to either the logging cable or tools from the limited H_2S exposure. Cycles and surfaces seen in the high-quality FMS data correlate well with conventional logs (gamma ray, sonic, and resistivity) and indicate the presence of high-frequency cycles (10–20 m thick) in the lower part

of the Quaternary–uppermost Pliocene succession. Simultaneous peaks on gamma-ray, resistivity, sonic, and susceptibility logs may reflect changes in sediment lithification throughout the logged section. Because of the high quality and uniform response of the sonic log, the WST was not deployed at this site. We anticipate that a check-shot survey at one of the other sites in this transect will provide appropriate drift control on the integrated sonic log.

Site 1128

Site 1128, the deep-water site of the Leg 182 shelf-to-basin transect, is located on the upper continental rise in 3874.4 m of water. The primary goals of this site were to (1) recover pelagic ooze from the upper continental rise to compile a paleoceanographic record of the Cenozoic opening of the Southern Ocean and development of the Circum-Antarctic Current, (2) determine the history of Cenozoic and Late Cretaceous CCD fluctuations and deep-water mass variations during the evolution of the Southern Ocean, and (3) determine depositional and diagenetic facies on the upper continental rise.

The sedimentary succession intersected at Site 1128 was divided into four major lithostratigraphic units. Unit I (0–95.6 mbsf) is a pink to brown, bioturbated, calcareous nannofossil ooze punctuated by numerous thin glauconite and planktonic foraminiferal sand calciturbidites and conglomeratic sediment gravity-flow deposits. A chaotic zone of debrites and slumped sediment (54.4–70.0 mbsf) separates this succession into three subunits containing variable proportions of resedimented material. Unit II (95.6–281.9 mbsf) is a thick section of uniform, green, variably calcareous clay and claystone that is locally interrupted, particularly in the upper parts, by several centimeter-thick turbidites composed of planktonic foraminiferal and nannofossil ooze. The relatively few carbonate particles in the sediment are etched and corroded, suggesting accumulation near the carbonate lysocline. The lower parts of this unit contain numerous well-preserved trace fossils (*Planolites, Chondrites, Zoophycos, Terebellina,* and *Thalassinoides*) and numerous thin chert horizons. A thin unit of green glauconitic sand to carbonate nannofossil ooze turbidites forms Unit III (281.9–284.0 mbsf) and marks a sharp change in sedimentation compared with the coarser, green, carbonate-free silts and clays of Unit IV (284.0–452.6 mbsf). Unit IV was subdivided into an upper Subunit IVA (284.0–358.4 mbsf) composed of bioturbated clayey siltstone with minor chert and glauconitic sand turbidites and Subunit IVB (358.4–452.6 mbsf) made up of pervasively burrowed sandy siltstone that grades to green silty sandstone at the base. The well-preserved siliceous microfossils and almost total lack of calcareous microfossils indicate accumulation below the CCD. The burrowed green sediment points to accumulation in dysoxic bottom waters.

Two major biostratigraphic successions were recovered at Site 1128 and dated by calcareous nannofossils and planktonic foraminifers as late Miocene–Quaternary (0–55 mbsf) and early Eocene–early Oligocene (72–427 mbsf). These intervals are separated by a debrite (55–72 mbsf) containing mixed upper Paleogene and Miocene nannofossils and planktonic foraminifers. Calcareous nannofossil data indicate four possible hiatuses within the Neogene succession, one of which is confirmed by planktonic foraminifer data at the upper/lower Pliocene boundary. A major unconformity beneath the debrite removed middle Miocene–upper Oligocene sediment (~15 m.y.). Below 72 mbsf, nanno-

fossils and planktonic foraminifers show increasing signs of dissolution and are absent at some levels, suggesting deposition near the lysocline and CCD. Sedimentation rates were 10–12 m/m.y. through the Neogene, 50–60 m/m.y. in most of the early Oligocene, and 4 m/m.y. in the late Eocene. Although characterized by poor core recovery and barren intervals, datum levels from the older Eocene succession suggest a sedimentation rate of 40–45 m/m.y. Five benthic foraminiferal assemblages are distinguished: (1) a diversified Quaternary and Pliocene assemblage indicating abyssal paleodepths above the CCD, (2) a mixed assemblage of displaced faunas in the debrites, (3) an impoverished lower Oligocene–lower upper Eocene assemblage indicating lower bathyal to abyssal paleodepths close to the lysocline, (4) an impoverished lower upper to upper middle Eocene calcareous assemblage indicating lower bathyal to abyssal paleodepths close to the lysocline, and (5) an impoverished upper middle to upper lower Eocene agglutinated assemblage indicating deposition below the CCD.

Long-core measurements established a magnetostratigraphy for the uppermost 40 mbsf, spanning the Brunhes Chron, Matuyama Chron, and part of the Gauss Chron. Below this, the interval characterized by debris flows disrupts the record, and it is not possible to recognize a magnetostratigraphy until a depth of ~60 mbsf, where the record was correlated with the early Oligocene magnetic polarity time scale. A nonmagnetic APC coring assembly was used at this site and produced significant improvement in the declination record in shallow APC cores. Excellent records were obtained both with and without the nonmagnetic assembly toward the bottom of the intervals cored by the APC.

Construction of a composite depth section from Holes 1128B and 1128C indicates that a complete Quaternary through upper Miocene sedimentary record was recovered at Site 1128. A break in the record occurs at ~68 mcd, corresponding to the 17-m-thick debrite separating upper Miocene from lower Oligocene sediments. The numerous turbidites in the section aided correlation. The primary lithologic parameters used to create the composite section were MS, gamma-ray attenuation (GRA), wet bulk density, NGR emissions data acquired by the multisensor track (MST) on whole cores, and color reflectance data (400 nm) measured on split cores.

Only low concentrations of methane were detected (maximum of 6.0 ppm), with most samples having less than 3 ppm. Calcium carbonate content has a bimodal pattern with generally high values (75–90 wt%) present in the upper 50 mbsf, followed by a decrease to a low of 2.1 wt% at 138 mbsf. Between 138 and 240 mbsf, carbonate content increases to a second mode with a maximum value of 68 wt%, and then decreases downhole with very low values (0–1 wt%) below 353 mbsf. Organic carbon concentrations are generally less than 0.16 wt% down to the base of Hole 1128B. Organic carbon values are 0 wt% from 200 to 276 mbsf, and headspace methane concentrations in this depth range are near background. Sulfur is present in only five samples in Hole 1128B, with values ranging from 0.05 to 0.21 wt%. Nitrogen is not detectable in any sample.

Site 1128 does not appear to be influenced by the high-salinity pore fluids observed at Sites 1126 and 1127. With the exception of the lower part of the cored interval, salinities are close to normal seawater values throughout. As a consequence of slow rates of deposition and low concentrations of organic material, pore fluids are not significantly depleted in sulfate in the upper sediments, and rates of carbonate recrystallization are relatively low. Two significant changes in pore-

water chemistry occur at Site 1128: the first at 20–40 mbsf, and the second between 236.8 and 253.3 mbsf. The change in pore-water chemistry at the shallow depth is manifest as an abrupt decrease in silica concentration from values of ~570 to 350 mM, corresponding to a slump unit. Seismic imagery indicates that this unit outcrops at the seafloor, so it is possible that bottom water has infiltrated the formation to cause this effect. The second major change in pore-water chemistry, accompanied by a decrease in salinity, is evident in most of the major and minor cations and occurs in the interval between lithostratigraphic Units II and IV. Concentrations of Mg^{2+}, K^{+}, SO_4^{2-}, and Na^{+} show a marked decrease, whereas Li^{+}, alkalinity, and Ca^{2+} increase. Although the change in salinity is accompanied by a decrease in Cl^{-}, this decrease is not of the magnitude expected from the salinity decrease alone, indicating that a portion of the salinity decrease is a result of the removal of cations and anions through precipitation and adsorption. Downhole logs indicate the presence of numerous relatively impermeable layers in the interval between lithostratigraphic Units II and IV, which would effectively limit vertical diffusion between these two units and allow them to geochemically evolve relatively independently of each other. The sediments in lithostratigraphic Unit IV contain very low concentrations of carbonate minerals, and reactions leading to the enrichment and depletions in the pore-water constituents principally involve clay minerals.

Sediment physical properties data at Site 1128 closely reflect lithologic variations observed in the recovered sediments and provide essential data for core-log correlation. Physical properties data were divided into five units on the basis of trends in the measured parameters. Physical properties Unit 1 (0–70 mbsf) is characterized by high variability in all datasets, corresponding to the lithologic sequence of turbidites and debris flows interbedded with nannofossil ooze. The base of this unit is marked by abrupt shifts in all parameters measured. Physical properties Unit 2 (70–139 mbsf) is characterized by low variability in all datasets, punctuated by a number of distinct data offsets (1–5 m thick) corresponding to sharply bounded intervals of redeposited nannofossil ooze. Physical properties Unit 3 (139–231 mbsf) is an interval characterized by relatively low and nearly constant values for all parameters, corresponding to a sequence of monotonous clays. An increase in NGR, MS, GRA, and discrete *P*-wave velocity and a decrease in porosity is observed at the upper boundary of PP Unit 4 (231–363 mbsf), below which all parameters display increased variability reflecting alternations of indurated and nonindurated sediments. The upper boundary of PP Unit 5 (363–452 mbsf) is marked by a negative shift in GRA, MS, and NGR, corresponding to the transition into lithostratigraphic Subunit IVB. Other than porosity, which decreases through the unit, the parameters measured show constant downhole trends for the remainder of the recovered interval.

Site 1128 was successfully logged with the triple combo and FMS/sonic tools. As a result of time constraints, the GHMT and WST tools were not run. Downhole logging data were divided into four units, with trends closely correlating with lithologic and sediment physical properties data. Logging Unit 1 (0–242 mbsf) is characterized by uniform values, punctuated by sharp decreases in gamma-ray values and increases in density and resistivity apparently corresponding to intervals of redeposited nannofossil ooze. Logging Unit 2 (242–295 mbsf) is characterized by high variability in all data sets, corresponding to an interval of high variability in sediment physical properties data and an interval of

variable lithification in cores. The lower part of this unit corresponds to lithostratigraphic Unit III and consists of nannofossil ooze interbedded with variably indurated sandstone turbidites. These interbedded sediments are reflected in logging data as alternations of low gamma-ray, high-density, and resistive intervals corresponding to calcite-rich layers, and high gamma-ray, low-density, and conductive intervals corresponding to sandstones. Logging Unit 3 (295–362 mbsf) has low variability and nearly constant values on all logs except the gamma ray, which increases downcore. Increased concentrations of thorium and potassium correspond to an increased concentration of terrigenous sediment. Logging Unit 4 (363–414 mbsf) has minimal variability in most parameters, with the exception of cyclic variations in gamma-ray values. Downhole measurements from Unit 5 indicate the presence of clays and quartz through the unit.

Site 1128 provided the first opportunity to sample and establish a seismic stratigraphy for this thick (containing more than 10 km of sediment) and laterally extensive continental rise basin. Seismic imagery shows that the thin (72 m), relatively condensed Neogene section (largely corresponding to lithostratigraphic Unit I) was deposited in a small perched sub-basin lying within a thick Paleogene and Mesozoic succession and that the Neogene sequence is thin or absent over much of the basin. Exposed Mesozoic sediments on the middle and lower slope are the presumed source of lithified material commonly present within resedimented intervals. Although not intersected because of operational time constraints, a prominent angular unconformity ~150 m below total depth at Site 1128 almost certainly marks the base of the Cenozoic succession. Apart from hiatuses between the lower and middle Eocene and the Oligocene and Miocene, Site 1128 results indicate that the upper part of this basin contains a thick, almost continuous biosiliceous record of Southern Ocean development through the Paleogene.

Site 1129

Site 1129 was the third and proximal site of a three-site transect through a set of upper Neogene clinoforms immediately seaward of the present-day shelf edge. Site 1129, located just seaward of the shelf edge in 202.5 m of water, intersects a more expanded record of the oldest part of the clinoform sequence. The principal objective of this transect was to collect detailed, high-resolution profiles through a late Neogene shelf edge (high energy) to upper slope (low energy) succession deposited within a cool-water carbonate environment, to determine the response of this type of depositional system to Pliocene–Quaternary sea-level fluctuations.

The succession recovered at Site 1129 is 604.2 m thick (Table T2) and was divided into three lithostratigraphic units. Unit I (0–149.8 mbsf) consists mainly of unlithified bryozoan floatstone to rudstone and bioclastic packstone to grainstone, with abundant bryozoan fragments. The floatstone and rudstone are pale yellow to light gray, with a poorly sorted, very fine to medium sand-sized bioclastic packstone matrix. The floatstone and rudstone contain abundant granule- to pebble-sized bryozoan fragments exhibiting highly diverse growth forms. The bioclastic packstone to grainstone is pale yellow, light gray, and light olive gray and consists of very fine to fine sand-sized bioclasts together with coarse sand- to granule-sized bryozoan fragments. The unit is divided into five subunits, each forming a package grading upward from bio-

clastic packstone at the base to bryozoan floatstone and rudstone at the top. We infer that each subunit represents an individual mound-building episode. Unit II (149.8–556.7 mbsf) consists of light gray, light olive gray, and gray bioturbated bioclastic packstone and minor grainstone and wackestone with four nannofossil chalk intervals. Lithification increases from unlithified sediments at the top of Unit II to partially lithified sediment with well-lithified chalk intervals at the base. The upper part of Unit II is dominated by very fine to fine sand-sized, generally well-sorted, massive bioclastic packstone with subordinate grainstone and wackestone. The lower part is characterized by muddy bioclastic mudstone, wackestone, and packstone with abundant well-defined burrows. Unit II therefore exhibits an overall coarsening-upward trend. Unit III (556.7–604.2 mbsf), with very poor recovery, consists of dolomitized, fine sand-sized bioclastic grainstone and chert fragments. It is likely that the chert fragments represent thin beds and lenses of preferentially silicified wackestone/ooze. The boundary between Units II and III is sharp and represents a major hiatus.

Site 1129 contains two biostratigraphic units: (1) an expanded Quaternary section more than 554 m thick that is underlain by a thin and conformable uppermost Pliocene section, and (2) a middle–lower Miocene section. These units are separated at 556 mbsf by an unconformity representing ~12 m.y., marked by a bryozoan turbidite overlying indurated sediments and chert layers. Calcareous nannofossils are generally abundant and moderately well preserved in the upper part of the section, but below 371 mbsf the preservation is poor. The preservation and abundance of planktonic foraminifers degrade more rapidly downhole than that of the nannofossil assemblages. Below ~68 mbsf, most characteristic features of foraminifers are obscured by carbonate cement and recrystallization. Benthic foraminifers are generally abundant and well preserved in the upper part of Hole 1129C. At a depth of ~140 mbsf, preservation and abundance deteriorate markedly. Three main assemblages are recognized at Site 1129: (1) a distinctive, well-preserved Quaternary assemblage found in bryozoan-rich accumulations (down to ~140 mbsf), (2) a Pleistocene–upper Pliocene assemblage (140–557 mbsf) that includes a variable redeposited neritic component, and (3) a sparse Miocene assemblage below ~560 mbsf. The two Quaternary–upper Pliocene assemblages indicate upper bathyal paleodepths, whereas the Miocene assemblage indicates an upper to middle bathyal paleodepth.

Long-core measurements of Hole 1129C sediments revealed an extensive interval of normal magnetization to a depth of ~340 mbsf. Sediments record reverse polarity magnetizations below that depth, with the boundary best defined by measurements on discrete samples. This reversal is interpreted as the Brunhes/Matuyama boundary. In Hole 1129D, a long interval of predominantly reverse polarity magnetizations to a depth of ~540 mbsf is interpreted as the upper part of the Matuyama Chron (C1r). The Jaramillo Subchron (C1r1n) is recorded in both holes at depths of ~400–440 mbsf. Normal polarities are recorded again in Hole 1129D at depths of 540–550 mbsf, possibly representing the Olduvai Chron (C2n). This would indicate a variable sedimentation rate, with the late Quaternary sedimentation rate nearly triple that of the early Pleistocene–latest Pliocene. Rock magnetic characteristics, such as near saturation with inductions of 400 mT and median destructive fields of the IRM of 20–40 mT, suggest that magnetite and possibly magnetic sulfides are the principal remanence carriers. ARM/IRM indi-

cate a high relative abundance of single-domain grains, possibly biogenic magnetite.

High concentrations of CH_4 and H_2S through much of the section are a major feature at Site 1129. Methane and H_2S concentrations at this site fall between the levels found at Sites 1127 and Site 1131. Calcium carbonate content is uniformly high, primarily in the range of 86–94 wt%. Organic carbon concentrations generally vary from 0.4 to 0.7 wt%.

Site 1129, like many other sites drilled during Leg 182, is influenced by the presence of high-salinity pore fluids within and below the cored interval. Within the cored interval, the presence of pore waters with Na^+/Cl^- ratios significantly higher than seawater indicates the influence of fluids that have been involved in the precipitation and dissolution of halite. Site 1129 was characterized by high rates of SO_4^{2-} reduction of organic material and consequent production of alkalinity. The absence of significant iron concentrations resulted in a pH less than 6. Although high concentrations of H_2S and high alkalinity values were measured at relatively shallow depths, significant SO_4^{2-} reduction did not occur until below 100 mbsf. This suggests that H_2S is diffusing from the underlying sediments into the overlying oxic sediments, where it is oxidized to SO_4^{2-}. Rates of carbonate alteration reflected in the Sr^{2+} concentration (>2 mM) were the highest yet observed during Leg 182. Dolomite is ubiquitous below a depth of 70 mbsf and reached values as high as 24 wt%.

Physical properties measurements at Site 1129 correlate well with lithologic changes observed in the sedimentary section and provide an important data set for core-log correlation. In general, Site 1129 is characterized by significant variations in NGR and GRA bulk density. In general, variations are less marked in *P*-wave velocity, porosity, and other physical properties data. A well-defined cyclicity is present in the NGR record and can be correlated with the downhole gamma-ray logs and NGR records from Site 1127 and 1131. Physical properties data were divided into three major units. Physical properties Unit 1 (0–40 mbsf) is characterized by a rapid increase in NGR, as observed at most other Leg 182 sites. The base of this unit coincides with the top of the three bryozoan mound sequences, which form the lower part of lithostratigraphic Unit I. *P*-wave velocity and bulk density also increase with depth toward the base of this unit. Physical properties Unit 2 (40–258 mbsf) is characterized by a uniformly high NGR with some cyclic variations and by a slight increase in GRA bulk density and *P*-wave velocity. A significant offset to higher values of *P*-wave velocity and bulk density can be seen at 90 mbsf in PP Unit 2. Physical properties Unit 3 (258–558 mbsf) is characterized by increasing *P*-wave velocity (1650–2450 m/s) and bulk density and decreasing porosity, which reflects the increasing induration of the succession. Below 558 mbsf, core recovery was too low for physical properties characterization of the deeper part of the sedimentary section.

Hole 1129D was successfully logged with three logging-tool strings. The triple combo produced very good results, except for the interval between 360 and 460 mbsf where the porosity log was affected by excessive borehole rugosity. The log patterns are very similar to those from Hole 1131A; the uranium gamma-ray log showed distinct cyclicity in the lower part of the Quaternary sequence with 18–20 individual cycles, each measuring 10–20 m in thickness. Chalk layers and firmgrounds in the Quaternary succession, as indicated by the conventional logs, are

clearly imaged by FMS data. The FMS data also provide a detailed picture of the thickness distribution of thinly bedded cherts (~20 cm) and carbonates (1–2 m) in the middle upper Miocene succession, where recovery was very poor.

The high-resolution site survey seismic data at Site 1129 clearly images the bryozoan mound complex within lithostratigraphic Unit I and shows that this or similar mound complexes have existed at and immediately below the shelf edge throughout the Pleistocene. A combination of the results from Sites 1129 and 1131, now correlated with the recognition of a distinctive motif on seismic data, confirms that development of extensive bryozoan mound complexes has been one of the characteristic features of Quaternary cool-water carbonate sedimentation across a large area of the western Great Australian Bight.

Site 1130

Site 1130 was located to intersect and characterize Neogene cool-water carbonate shelf edge sequences and the nearshore portion of a Paleocene?–middle Eocene progradational siliciclastic wedge (seismic Sequences 2, 4, and 6A). The principal objectives were to (1) recover a detailed record of siliciclastic progradation and aggradation to evaluate the complex interaction among Paleogene sea-level fluctuations, accommodation space, and subsidence; (2) determine the facies characteristics, sea-level response, and paleoceanographic history of a Neogene cool-water carbonate succession in a shelf edge setting; and (3) evaluate diagenetic history and processes within the Neogene facies in a shelf edge setting.

The sediments recovered at Site 1130 were divided into four major lithostratigraphic units. Unit I (0–261.43 mbsf) is a light gray to pale olive, strongly bioturbated, unlithified to partially lithified bioclastic packstone. This succession is punctuated by unlithified bioclastic wackestone layers and occasional nannofossil foraminiferal ooze to chalk intervals. The upper part of this unit is characterized by a repetitive uphole textural change from matrix-supported to grain-supported sediment. Lighter intervals in the otherwise monotonous packstones are fine grained and foraminifer rich, whereas the generally coarser and darker intervals contain more bioclasts. The lower part of Unit I is typified by gradual color changes ranging from light gray to olive gray with a few abrupt transitions. Soft sediment deformation structures interpreted as slumps are present at the base of Unit I. Unit II (261.43–328.86 mbsf) is dominated by strongly bioturbated, white to light gray nannofossil foraminiferal chalk with a wackestone to packstone texture. Disseminated black grains (pyrite, glauconite, and other unidentifiable grains) are scattered throughout the unit. Unit III (328.86–369.50 mbsf) consists of chert layers (silicified nannofossil planktonic foraminiferal ooze) interbedded with intervals of white nannofossil planktonic foraminiferal ooze. The light to dark gray, partially translucent chert fragments contain burrows filled with white, fine-grained, lithified planktonic foraminiferal packstone to grainstone. Unit IV (369.50–386.51 mbsf) is dominantly a calcareous sandstone, but with compositional and textural variability encompassing red bioclastic glauconitic wackestone; sandy bryozoan grainstone; pink, coarse-grained bivalve grainstone; and red, very coarse grained calcareous sandstone.

Calcareous nannofossils and planktonic foraminifers indicate that three biostratigraphic successions were recovered at Site 1130: (1) Quaternary–upper Miocene (0–327 mbsf), (2) upper–middle Oligocene

(327–~355 mbsf), and (3) a sandy limestone of unknown age from the bottom of Holes 1130A and 1130C. Preliminary results indicate that the upper part of the lower Pliocene is missing (>1 m.y.) and that the major disconformity between upper Miocene and Oligocene sediments represents a hiatus of at least 15 m.y. The sedimentation rate for the middle–upper Oligocene was 10–30 m/m.y., although this should be viewed with caution because of poor core recovery. The rate fluctuated between 15 and 30 m/m.y. during the Pliocene–Miocene and reached as high as 240–260 m/m.y. during most of the Quaternary. The three benthic foraminiferal assemblages recognized correspond respectively to the Oligocene, early Pliocene–late Miocene, and Quaternary–late Pliocene, and indicate a shallowing-upward trend during these time periods. The Oligocene and lower Pliocene–upper Miocene assemblages are typically cosmopolitan, middle bathyal assemblages, whereas the Quaternary–upper Pliocene contains a mixed assemblage representing upper bathyal paleodepths and containing many well-sorted specimens from shelf environments.

Long-core measurements revealed an extended interval of normal magnetization and then a sharp reversal to normal polarity at 199.9 mbsf, interpreted as the Brunhes/Matuyama boundary. Intensities of magnetization varied from 0.01 to 1 mA/M with an overall decreasing trend downhole. Within this general trend are fluctuations with dominant wavelengths of a few tens of meters. The ratio of ARM/IRM, a measure of the relative importance of single-domain to multidomain behavior, decreases downcore, suggesting that the role of biogenic magnetite diminishes. Coupled with the decrease in magnetization, this strongly suggests that fine-grained magnetite of biogenic origin is preferentially dissolved.

An experimental nonmagnetic cutting shoe was used for alternate cores between Cores 182-1130A-3H and 7H, and an entire nonmagnetic core-barrel assembly was used on Cores 182-1130B-3H to 7H. Both the nonmagnetic shoe and core-barrel assembly produced reductions in radial component contamination, but the effects were not as dramatic as at Site 1128.

Construction of the composite section from Holes 1130A and 1130B indicates that a continuous sedimentary record was not recovered at Site 1130. Low recovery in Core 182-1130A-3H and no recovery in Core 182-1130B-3H produced a gap at 22–24 mbsf. The record below this is apparently continuous to ~191 mcd (all Quaternary), at which depth core overlap becomes minimal to nonexistent, disrupting continuity of the spliced section. The primary lithologic parameters used for correlation at Site 1130 were NGR emissions and the 700:400 nm ratio of color reflectance data.

Only low concentrations of CH_4 were detected, with most samples containing <7 ppm (maximum = 11.3 ppm). Calcium carbonate content ranges from 80.9 to 93.2 wt% in lithostratigraphic Units I and II, with most samples varying between 85 and 90 wt%. No carbonate analyses were conducted in Units III and IV (328.9–386.51 mbsf) because of low core recovery.

Site 1130 is influenced by high-salinity pore fluids, as was the case at Sites 1126 and 1127. The maximum rate of salinity increase, 5.7/m, is the highest observed during Leg 182. The steep gradient down to ~32 mbsf and then the constant salinity concentration (83) below suggest nonsteady-state conditions. In contrast to Site 1127, the SO_4^{2-} reduction zone is incomplete and confined to the upper part of the profile,

and the degree of SO_4^{2-} reduction is ~40% less than at Site 1127. These differences are probably caused by a lower initial organic carbon content at Site 1130. As a consequence of the decreased sulfate reduction activity, interstitial waters are saturated with respect to $SrSO_4$ (celestite), limiting pore-water Sr^{2+} concentrations.

Sediment physical properties data closely reflect Oligocene–Holocene lithologic variations observed in recovered sediments and downhole logging data. Three physical properties units were recognized, primarily on the basis of trends in NGR. The homogenous bioclastic packstones of PP Unit 1 (0–43 mbsf) are characterized by low variability in all measured parameters. The large increase in NGR from 5 to 35 cps at the base of PP Unit 1 does not correlate to any lithologic change but is roughly coincident with an increase in *P*-wave velocity variability, suggesting that it results from diagenesis. Physical properties Unit 2 (43–254 mbsf) is dominated by cyclic variations in NGR that appear to be related to Milankovitch cyclicity on a 100-k.y. frequency from 43 to 175 mbsf and on a higher 41-k.y. frequency for the remainder of the unit. This change in frequency occurs near the Brunhes/Matuyama boundary and is clearly seen in downhole logging data from this site. From 199 to 254 mbsf in PP Unit 2, increased variability in *P*-wave velocity reflects the presence of a series of firmgrounds observed in the recovered sedimentary section. The upper boundary of PP Unit 3 (254–335 mbsf) correlates well with a distinct change in lithology (lithostratigraphic Unit II) from packstone/wackestone to nannofossil oozes and chalks. NGR and *P*-wave velocity show low variability within PP Unit 3, whereas bulk density shows a general increasing trend.

Three large-scale units were identified in downhole logging data from Hole 1130C, based on shifts in conventional and FMS logs, with boundaries at 258 and 329 mbsf. The interval above 258 mbsf is characterized by a near-constant background level of gamma radiation of 20 American Petroleum Institute (API) units, with individual spikes reaching 40–45 API. The boundary at 260 mbsf is defined at a sharp downhole decrease in the uranium gamma-ray log, and the boundary at 329 mbsf corresponds to the change from carbonate sediments above to siliciclastic deposits below.

Integration of the various data sets with the regional seismic stratigraphic interpretation provides a sequential record consisting of the seismic Sequence 7 Eocene? progradational wedge deposited at shelf water depths; overlain after an indefinite hiatus by deep-water, seismic Sequence 6A upper Oligocene oozes that have since been irregularly silicified. The record then contains another hiatus of ~20 m.y., before deposition of upper Miocene–lower Pliocene seismic Sequence 3 oozes, capped by a packstone unit, as a continuation of a shallowing-upward trend. A further short hiatus was then followed by rapid deposition of a thick sequence of seismic Sequence 2 Quaternary wackestones and packstones at upper slope/shelf edge depths.

Site 1131

Site 1131 was the second and intermediate site of a three-site transect through a spectacular set of upper Neogene clinoforms immediately seaward of the present-day shelf edge. Site 1131, located on the upper slope in 332.4 m of water, intersected a more expanded record of the middle part of the clinoform sequence. The principal objective of this transect was to collect detailed, high-resolution profiles through an

upper Neogene shelf edge (high energy) to upper slope (low energy) succession deposited within a cool-water carbonate environment, and to determine the response of this type of depositional system to Pliocene–Quaternary sea-level fluctuations.

Three major lithostratigraphic units were identified at Site 1131. Unit I (0–25.0 mbsf) consists dominantly of bioclastic packstone, floatstone, and rudstone. The upper part of Unit I is composed of a massive, homogeneous, light gray to olive gray, unlithified bioclastic packstone that includes a significant bryozoan component. The lower part of Unit I is a heterogeneous interval of unlithified bryozoan floatstone and rudstone punctuated by thin (decimeter scale) layers of wackestone, packstone, and grainstone. Unit II (25.0–531.7 mbsf) consists of a very thick (>500 m), homogeneous succession of light gray to olive-gray bioclastic packstone, grainstone, and wackestone. In general, lithification and diversity of the bioclastic component increase downhole. Unit III (531.7–607.4 mbsf) is separated from Unit II by an unconformity representing a major hiatus. Below the unconformity, recovery was incomplete in a succession consisting of dark gray, silicified nannofossil ooze beds or lenses within olive-gray partially to strongly lithified bioclastic grainstone containing blackened grains and glauconite.

Two biostratigraphic successions were identified at Site 1131: (1) an expanded Quaternary interval more than 510 m thick underlain by a thin and conformable uppermost Pliocene interval and (2) a middle and lower Miocene section lacking hiatuses within the resolution of available biostratigraphic data. These successions are divided by a disconformity at 532 mbsf that spans ~10 m.y. An environmental crisis produced an unusual nannofossil assemblage dominated by *B. bigelowii* near the base of Zone NN19 at ~522 mbsf. A similar event was observed in the same stratigraphic interval at Site 1127. Carbonate microfossils, especially foraminifers, were strongly affected by overgrowths, cementation, and recrystallization below 60–100 mbsf. These effects are consistent with the pore-water geochemistry and the onset of lithification. One main Quaternary–uppermost Pliocene upper bathyal assemblage of benthic foraminifers is recognized above 100 mbsf. This assemblage also contains a large proportion of small neritic tests (63–150 µm), probably redeposited from the shelf. Well-preserved benthic foraminifers, including a high proportion of large specimens (>1 mm), are found together with well-preserved bryozoans down to 25 mbsf. Poor preservation prevented detailed faunal analysis below 100 mbsf.

Magnetic measurements of archive-half cores established a magnetostratigraphy to a depth of 320 mbsf, which includes the Brunhes and uppermost Matuyama Chrons. Below this, drilling disturbance disrupted the record and no further magnetostratigraphic data were obtained. Rock magnetic properties show minimum downhole variability and are consistent with single-domain biogenic magnetite, except for cores between 70 and 150 mbsf that display the typical behavior of ultrafine-grained (superparamagnetic) greigite. Magnetic susceptibility is dominated by contributions from the diamagnetic carbonate matrix.

Composite section construction from Holes 1131A and 1131B indicates that a continuous record was not recovered. Overlap between cores in adjacent holes was maintained to ~55 mcd, until poor recovery in Core 182-1131C-6H resulted in a short (few centimeters) data gap. Below 70 mbsf, low recovery from extended core barrel cores resulted in reduced core overlap and prohibited splicing below 78 mcd. The primary parameters used for correlation were NGR emissions, GRA bulk

density, and color reflectance. Comparison of data between holes revealed a low degree of similarity, making correlations difficult.

The most striking organic geochemical results from Site 1131 were the high concentrations of CH_4 and H_2S in the upper part of the section. In comparison to Site 1127, gas pockets were less abundant, and the concentration of CH_4 in both gas pockets and headspace samples at Site 1131 was lower. Hydrogen sulfide concentrations, however, were comparable at both sites. Atypically, C_1/C_2 ratios first increase then decrease with increasing depth in Hole 1131A, essentially mirroring the methane profile as C_2 varies little throughout the section. Calcium carbonate content is uniformly high (86–94 wt%). Organic carbon is less than 0.4 wt% down to 125 mbsf, with higher values (as much as 1.0 wt%) at greater depths.

Site 1131 exhibited inorganic geochemical features similar to those at Site 1127, with the exception of more extreme changes in pore-water geochemistry profiles because of increased degradation of organic material. For example, alkalinity reached a maximum value of 137 mM, compared to 106 mM at Site 1127. In contrast to Site 1127, although there was significant depletion in the concentration of SO_4^{2-}, measurable concentrations remained even in the zones of highest alkalinity, suggesting that organic material was the limiting factor in the production of H_2S at Site 1131. Excess SO_4^{2-} in the upper portion of the core suggests that the oxidation of H_2S originated lower in the section. In the upper 300 m, depletion in the concentrations of Ca^{2+} and Mg^{2+} and enrichment in Sr^{2+} indicate a recrystallization of aragonite and HMC. This was confirmed by mineralogical analyses, which showed that HMC had disappeared by 50 mbsf. Aragonite gradually decreased with increasing depth and vanished at the Pliocene/Pleistocene boundary. Ratios of Na^+/Cl^- were in excess of the ratio in seawater throughout the Quaternary section, indicating that the high-salinity fluids had participated in the precipitation and dissolution of halite.

Physical properties measurements at Site 1131 correlate well with lithologic changes observed in the sedimentary section and provide the basic data for core-log correlation to reconstruct poorly recovered intervals. Correlation of downhole gamma-ray logs with NGR data from the MST indicates that moderate to poor recovery at Site 1131 may have aliased and concealed in cores the cyclic fluctuations that are clearly visible on downhole logs. Physical properties data indicate that the cored interval is divisible into two units. Physical properties Unit 1 (0–31 mbsf) is mainly defined by a large increase in NGR toward the base of the unit, corresponding to the lower limit of the bryozoan floatstone/rudstone comprising lithostratigraphic Subunit IA. This NGR peak is also observed on downhole logs, with spectral gamma data indicating that it reflects uranium content and, accordingly, is either the result of increased organic matter content or carbonate diagenesis. *P*-wave velocity and bulk density also increase toward the base of this unit. Physical properties Unit 2 (31–532 mbsf) is characterized by gradual increases in porosity, *P*-wave velocity, and bulk density, primarily reflecting increased compaction, but also showing data excursions corresponding to coarser and more lithified horizons. More indurated layers within the generally homogenous sediments of PP Unit 2 have increased velocities and bulk densities and generally lower NGR. Below 532 mbsf, core recovery was too low for physical properties characterization of the deeper part of the sedimentary section.

Three logging-tool strings were deployed in Hole 1131A. Downhole logging data indicate that the uppermost part of the cored section (0–28 mbsf) correlates with bryozoan-rich horizons described in core. As was noted with the physical properties data, a uranium peak at the base of this unit reflects increased organic content and/or carbonate diagenesis and may represent a firmground. The remainder of the cored section to 575 mbsf contains porosity-density crossovers that coincide with low PEF values and high resistivity and sonic values. These crossovers are interpreted as probable chert layers. In contrast, low-porosity peaks associated with density, PEF, sonic, and resistivity peaks may represent possible firmgrounds.

Integration of coring results with high-resolution site survey seismic data at Site 1131 confirms that the mounded features visible in the uppermost part of the seismic section are in fact bryozoan-dominated mounds. The spectacular clinoform geometry corresponding to the remainder of the cored interval consists of bioclastic packstone, grainstone, and wackestone, with variable lithification as the dominant factor controlling seismic data amplitude and impedance variability. The lithostratigraphic and biostratigraphic boundary toward the base of the section coincides with a major regional unconformity and the base seismic Sequence 2 sequence boundary.

Site 1132

Site 1132 was located to intersect and characterize Neogene cool-water carbonate shelf edge sequences and the nearshore portion of a Paleocene?–middle Eocene progradational siliciclastic wedge (seismic Sequences 2, 3, 4, and 6A). The principal objectives were to (1) recover a detailed record of siliciclastic progradation and aggradation to evaluate the complex interaction among Paleogene sea-level fluctuations, accommodation space, and subsidence; (2) determine the facies characteristics, sea-level response, and paleoceanographic history of a Neogene cool-water carbonate succession in a shelf edge setting; and (3) evaluate the diagenetic history and processes within the Neogene facies in a shelf edge setting.

The recovered succession was divided into six lithostratigraphic units. Unit I (0–113.5 mbsf) consists of bryozoan floatstone and rudstone, alternating with bryozoan packstone and, in the lower part, also bioclastic wackestone with bryozoans. The abundant bryozoan fauna are highly diverse and include a great variety of growth forms. The sediments are unlithified and burrow mottled, and the color is dominantly light gray with thinner pale olive and white intervals. This unit represents a major bryozoan mound complex. Unit II (113.5–158.3 mbsf) consists of uniform bioclastic packstone with a great diversity of bryozoan growth forms. The color is light gray, with minor light olive gray and white intervals. The sediment is burrow mottled and mainly unlithified, but thin, partially lithified beds are present between 130 and 140 mbsf. Unit III (158.3–250.70 mbsf) consists of unlithified bioclastic packstone and minor wackestone and grainstone, with an interbedded thin package of foraminiferal ooze and chalk. The unit is strongly burrowed and mainly unlithified down to 168 mbsf and partially lithified below that level. The color is dominantly light olive gray with thinner olive, pale olive, and white intervals. Several prominent firmgrounds are the basis for subdivision into five subunits. Unit IV (255.80–437.33 mbsf) was poorly recovered; however, available data suggest that it consists of bioclastic packstone and grainstone with an interval of nanno-

fossil foraminiferal chalk partially replaced by nodular, light to dark gray chert. Unit V (441.50–517.70 mbsf) is also characterized by poor recovery, but recovered material indicates that it consists of bioclastic packstone and grainstone and lacks chert. Glauconite is abundant, and the colors vary between very pale brown and pale yellow. Unit VI (517.70–555.95 mbsf) is topped by a prominent mineralized hardground and consists of lithified bioclastic packstone and wackestone. It differs from overlying units in its color, prominent firmgrounds and hardgrounds, solution seams, and centimeter-sized bioclasts. The color is pale yellow at the top and passes downward into light gray, pale yellow, red yellow, to pale red and dark red at the bottom. The lowest recovered bed contains pebbles of siliciclastic sandstone rich in lithic fragments.

Calcareous nannofossils and planktonic foraminifers indicate that drilling at Site 1132 recovered a thick Quaternary–Eocene sequence (~550 m thick) overlying a relatively thin, barren section (~45 m). Calcareous nannofossils from the basal Quaternary–uppermost Pliocene unit registered a nannofossil event, the "*Braarudosphaera* Event" previously recorded at Sites 1127, 1130, and 1131, indicating a dramatic short-lived change in surface-water conditions over a large geographic area. The thick Quaternary–uppermost Pliocene section (~235 m) contains combined Zones NN21–NN20 and Zone NN19, and the thick middle Miocene section (~300 m) contains Zones NN6 and NN5–NN4. These sections are separated by a thin interval (~20 m) with poor core recovery. Hiatuses are likely within this thin interval, where the recovered nannofossils and planktonic foraminifers suggest late Miocene age. Another similarly thin interval (~20 m) with poor core recovery, which is also likely to contain hiatuses, is recorded between the middle Miocene section and the underlying mainly lower Oligocene section. Fossils of early Miocene age were reported in this condensed unit. An Eocene age is indicated for the section underlying the lower Oligocene, based on thin-section analysis of two samples at ~530 and ~547 mbsf, respectively. A sharp change in sedimentation rates corresponds to the condensed interval between Quaternary–upper Pliocene and middle Miocene sections. The Quaternary–uppermost Pliocene section registered an average sedimentation rate of 175 m/m.y., whereas the middle Miocene showed an average rate of 20 m/m.y. Another condensed section between the middle Miocene and Oligocene successions is indicated by the sparse biostratigraphic datums through this interval. Four main benthic foraminiferal assemblages are identified. These indicate an upper to middle bathyal paleodepth for the Pleistocene–Oligocene section. In the Pleistocene, a striking, well-preserved assemblage characterized by many large (>1 mm) agglutinated foraminifers is found within bryozoan-rich accumulations. This assemblage probably reflects a diverse, highly dynamic ecosystem that became established at the seafloor at various times during the Quaternary, corresponding to episodes of bryozoan mound growth. Changes in the composition of this assemblage may relate to sea-level or circulation fluctuations.

The Brunhes/Matuyama boundary was found at ~180 mbsf, yielding a sedimentation rate of ~230 m/m.y. above this level. There were indications of the same intensity fluctuations observed at earlier sites; therefore, there is a possibility of high-resolution stratigraphy within the Brunhes Chron after further shore-based work. The top of the Jaramillo Subchron was found at 230 mbsf, which is consistent with this sedimentation rate. Magnetic anomalies were found associated with hardgrounds with mineralized crusts and with lithified skeletal

limestones. In some cases, this suggests that diagenesis occurred extremely early, within 100,000 yr after deposition.

As at Sites 1126, 1128, and 1130, only low concentrations of CH_4 were detected at Site 1132. Of the four sites, Site 1132 has the highest CH_4 content, with a maximum value of 54 ppm. Unlike the other low-methane sites, H_2S is present at Site 1132 in low concentrations. Calcium carbonate content is between 85 and 95 wt%, with values at the higher end of the range near the surface and declining gradually toward the lower end of the range with depth. Organic carbon values are primarily in the range of 0.3–0.6 wt%. Nitrogen concentrations are all less than 0.1 wt%, and sulfur is present at low concentrations in only a few samples in the upper 90 mbsf.

Site 1132 is influenced by the presence of high-salinity fluids, as is the case with all previous Leg 182 sites except 1128. However, unlike the adjacent Site 1130, the rate of salinity increase with depth is uniform and shows no evidence of nonsteady-state conditions. Site 1132 possibly had an initially higher organic carbon content, producing slightly higher SO_4^{2-} reduction rates and a more extended SO_4^{2-} reduction zone. As a result, carbonate diagenesis is more active, causing carbonate precipitation in the upper part of the profile, whereas the lower part is characterized by carbonate dissolution. As with Site 1131, Site 1132 displays a Na^+/Cl^- anomaly in the upper part of the profile. Site 1132 is characterized by a constant seawater composition of both conservative and nonconservative interstitial water constituents in the upper 30 mbsf, suggesting active flushing with seawater. With the completion of the slope transect from Site 1130 to 1132, we can draw initial conclusions about the horizontal distribution of brine in this area. It appears that salinity values at Sites 1130 and 1132 stabilize at about the same depth below the sea surface, suggesting a horizontal top of the main brine body at ~520 mbsl.

High-quality NGR and GRA bulk density data were obtained from the MST. Variations of NGR and GRA bulk density, supplemented by index properties measurements of porosity and thermal conductivity, form the basis for the five physical properties units recognized at Site 1132. Physical properties Unit 1 (0–5 mbsf) is characterized by very low (<5 cps) NGR and a high initial bulk density (>1.9 g/cm^3), which declines rapidly with depth. This unit corresponds to a thin package of grainstones that caps lithostratigraphic Unit I. Physical properties Unit 2 (5–140 mbsf) displays an overall increase in bulk density with depth (1.65–1.90 g/cm^3). There is a corresponding decrease in porosity from 55% to 43%, but with considerable variation probably associated with lithologic variability. High-amplitude cyclic variation in both NGR (>20 cps) and bulk density (0.2 g/cm^3) is also observed throughout this unit. Physical properties Unit 3 (140–248 mbsf) is characterized by a decline with depth in GRA bulk density and porosity and by a continued but more regular cyclicity in both NGR and GRA bulk density. Physical properties Unit 4 (~248–520 mbsf) is recognized solely on the basis of a change in NGR from 25 to <5 cps at 248 mbsf. Similar characteristics are present in limited core recovery from 516 to 520 mbsf, with cherts showing the anticipated high values of *P*-wave velocity. Physical properties Unit 5 (>520 mbsf) is poorly characterized because of limited recovery and drilling disturbance. NGR shows a shift back to higher values (10–20 cps), but there are considerable fluctuations associated with the much greater variety of lithologies present.

Two logging runs were attempted at Site 1132. The triple combo successfully logged 560 m, whereas hole conditions limited the FMS/sonic tool to only 70 m. Logging data closely reflect lithologic variations observed in the upper 245 mbsf of the section. Below this depth, downhole logs enable the characterization of sedimentary sequences in low recovery intervals and assist in intersite correlations. Logging data were divided into four units on the basis of variations in the collected datasets. Logging Unit 1 (0–242 mbsf) is characterized by an increase in the magnitude and variability of gamma-ray values that are mainly the result of increased uranium concentrations. High and variable uranium contents continue for the remainder of the unit, with an abrupt decrease at the boundary with logging Unit 2. In the open-hole logged interval below 104 mbsf, separation of the porosity and density curves indicates a somewhat higher noncarbonate fraction than is present higher in the hole. This noncarbonate fraction is only slightly enriched in K and Th. The base of logging Unit 1 correlates well with the base of lithostratigraphic Unit III. Logging Unit 2 (242–437 mbsf) is characterized by a return to low gamma-ray values and increased variability in the magnitude of density and porosity variations, possibly caused by chert layers. In addition, resistivity logs from logging Unit 2 indicate that drilling fluid invasion occurred within this partially lithified packstone interval, suggesting higher porosity than in surrounding units. In the lower part of logging Unit 2, both porosity and density values increase, as does the degree of fluid invasion. The base of logging Unit 2 correlates well with the base of lithostratigraphic Unit IV and is characterized by increases in resistivity and decreases in gamma-ray values, porosity, and density. Logging Unit 3 (437–524 mbsf) is characterized by nearly constant density and gamma-ray values and variable porosity. Resistivity logs show low variability and indicate that drilling fluid invasion occurred in this interval, although to a lesser extent than in the units above and below. Logging Unit 3 correlates well with lithostratigraphic Unit V, which, despite low recovery, appears to be dominated by a homogenous interval of lithified bioclastic grainstones. The upper boundary of logging Unit 4 (524–537 mbsf) is marked by a sharp increase in all parameters. Within the limited section logged, resistivity measurements show increased drilling fluid invasion. The gamma-ray increase in logging Unit 4 is dominated by increased Th and K, indicating the presence of terrigenous minerals within the carbonate sediments. Logging Unit 4 correlates with lithostratigraphic Unit VI.

Regional seismic stratigraphic correlation shows that the Quaternary bryozoan mound complex, represented on seismic imagery by a distinctive mounded facies, occurs in a narrow band immediately below the shelf edge along much of the western Great Australian Bight. Lithostratigraphic data indicate that bryozoans are also important constituents of underlying nonmounded packstone and grainstone facies corresponding to the lower parts of seismic Sequence 2. Seismic Sequences 3 (middle–late Miocene) and 4 (early Miocene) are characterized by bioclastic grainstones, packstones, and wackestones, with minor foraminiferal ooze. Increased amplitudes toward the base of Sequence 3 probably represent increased impedance contrast associated with interbedded silicified horizons, and disconformity surfaces visible on the high-resolution seismic within both sequences appear to correlate with firmgrounds and hardgrounds. Lithostratigraphic and biostratigraphic data show that the small mounds immediately overlying the distinctive Sequence 7 progradational wedge are composed of lithified bioclastic packstone and wackestone of Eocene age. The only samples recovered

from Sequence 7 are carbonate-cemented sandstone fragments forming the uppermost sequence boundary, with the underlying friable sandstones being too poorly cemented for recovery.

Site 1133

Site 1133 is located on the middle upper slope in 1037.2 m of water. It was one of two paleoceanographic sites located to intersect pelagic sections that collectively span the entire Cenozoic succession and form the deeper water component of the shelf-to-basin transect. The principal objectives at this site were to (1) recover pelagic ooze from the middle upper slope to construct a Cenozoic paleoceanographic record of the opening of the Southern Ocean and the development of the Circum-Antarctic Current, (2) determine the history of Cenozoic CCD fluctuations and intermediate water mass variations, and (3) determine depositional and diagenetic facies on the middle upper slope. Drilling difficulties severely restricted the extent to which these objectives could be met.

Sediments recovered at Site 1133 were divided into two major lithostratigraphic units. Unit I (0–28.55 mbsf) consists of gray and white, moderately to strongly bioturbated calcareous ooze with varying amounts of calcareous nannofossils and planktonic foraminifers. This unit was divided into three subunits based on color changes, textural differences, firmgrounds, and a scoured surface. The boundary between Unit I and II is marked by a firmground that separates overlying white nannofossil ooze from underlying unlithified bioclastic wackestone. Unit II (28.55–142.59 mbsf) consists mainly of (1) gray to light gray, poorly sorted, unlithified bioclastic wackestone, with very fine grained silt- to sand-sized particles; (2) gray, light gray to light olive-gray, unlithified to partially lithified bioclastic packstone with poorly to well-sorted silt- to sand-sized grains; and (3) gray to dark gray chert/porcellanite (silicified wackestone). Most of the recovered sediments are pebble- to cobble-sized fragments. Some porcellanite/chert fragments are draped with a thin layer of unlithified to partially lithified bioclastic packstone. It is likely that the entire unit consists of bioclastic packstone or wackestone containing beds or lenses of preferentially silicified limestone (formerly nannofossil planktonic foraminiferal ooze/chalk).

Drilling at Site 1133 revealed the presence of two major biostratigraphic units, dated by nannofossils and planktonic foraminifers as Quaternary and middle–early Miocene. The Quaternary sequence extends down to 21.49 mbsf and overlies a thin, highly condensed interval with upper Miocene assemblages. This disconformity represents a hiatus of at least 3 m.y., and a second disconformity at 28.55 mbsf separates upper Miocene from lower–middle Miocene sediment and spans ~6 m.y. Three main benthic foraminiferal assemblages are recognized—a diversified Quaternary calcareous assemblage, a diversified upper Miocene assemblage, and an impoverished middle–lower Miocene assemblage. All three assemblages indicate middle to lower bathyal paleodepths.

Magnetic measurements of archive-half cores establish a tentative Quaternary–late Pliocene? magnetostratigraphy to 40 mbsf in Hole 1133B, which includes the Brunhes Chron (0–12 mbsf), Matuyama Chron (12–24 mbsf), and Gauss Chron (24–? mbsf). The interpretation is problematic because the same result was not reproduced in Hole 1133A, which yielded uniform normal polarity magnetizations to a depth of 20 mbsf and anomalously shallow magnetizations of both

polarities below this depth. Intensities are low; after demagnetization to 20 mT, median values are ~7×10^5 A/m. Intensity fluctuations are closely correlated with lithology in both holes but appear to be inversely correlated with MS. Anomalously high intensities and susceptibilities are observed in both holes at ~30 mbsf. Rock magnetic properties are consistent with single-domain biogenic magnetite or greigite as the remanence carrier. Magnetic susceptibility is dominated by contributions from the diamagnetic carbonate matrix.

Construction of the composite and spliced section from Holes 1133B and 1133C indicates that a complete record of the cored interval between 0 and 39 mcd (34 mbsf) was recovered. This depth interval includes sediments of Quaternary–early Miocene age. Distinctive high-amplitude events occur in the reflectance and GRA density records, enabling easy correlation between holes. Difficulties in correlation result from a slumped interval at ~20–32 mcd; however, the base of the slumped interval is clearly defined and provides a good correlation horizon.

Except for two samples with slightly higher methane contents, generally low concentrations of methane (<12 ppm) were detected at Site 1133. Calcium carbonate content ranges from 78.5 to 94.4 wt%, with most samples between 85 and 92 wt%. Organic carbon values are <0.4 wt%.

Seven interstitial water samples were collected at Site 1133. These data indicate that Site 1133 may be, as was the case with most other sites, underlain by high-salinity fluids, although the maximum salinity value measured was 41 at 123.4 mbsf. Compared to shallower sites, the sulfate reduction rate is substantially reduced and the resulting maximum alkalinity values are <5.2 mM. This, together with the small variations in excess calcium, suggests that the rate of carbonate diagenesis is slower than at other Leg 182 sites in shallower water.

Physical properties measurements at Site 1133 were limited because of poor core recovery. Data were divided into two units, with the boundary correlating with the base of the Quaternary section. Physical properties Unit 1 (0–21.8 mbsf) is characterized by increasing NGR (5–22 cps), bulk density (1.65–1.95 g/cm^3), velocity (1.57–1.62 km/s), and decreasing porosity (62%–45%). At the top of PP Unit 2, NGR values decrease to 5 cps, bulk density decreases to 1.8 g/cm^3, and porosity shows a general increase to 58%. Physical properties Unit 2 (21.8–152.1 mbsf) is mainly composed of neritic carbonate with low NGR values (~5 cps), variable density, and variable velocities, correlating with an alternation between high-velocity silicified limestones and packstones and lower velocity partially lithified/unlithified packstones.

Regional seismic stratigraphic correlation shows that the youngest interval, of Quaternary age, corresponds to seismic Sequence 2. The remainder of the succession corresponds to seismic Sequence 3. The hiatus recognized at 28.55 mbsf correlates with one of the intrasequence disconformities apparent on the high-resolution site-survey seismic data.

Site 1134

Site 1134 is located on the eastern Eyre Terrace upper slope in 701.0 m of water. This site was designed to intersect Cenozoic seismic Sequences 2, 3, and 4 and Lobes 2 and 3 of Sequence 6A (Feary and James, 1998, reprinted as **Chap. 2**), and as much of the upper part of the Cretaceous section as time permitted. The principal objectives at this site

were to (1) collect a detailed record of Paleogene–early Neogene temperate to subtropical midlatitude sedimentation in an upper slope environment and (2) recover a record of marine flooding of the evolving rift basin in the Cenomanian. The target depth at this site was just below a high-amplitude reflector of probable Cenomanian age, estimated before drilling to be at 520 mbsf (on the basis of stacking velocities).

Site 1134 contained a 397.1-m-thick succession (Table T2) of Quaternary–middle Eocene sedimentation that was divided into six units. Unit I (0–33 mbsf) consists of calcareous nannofossil ooze with varying amounts of planktonic foraminifers. In general, whitish matrix-supported intervals consisting of planktonic foraminifers, sponge spicules, bioclasts, benthic foraminifers, radiolarians, and minor tunicate spicules in the >63-µm fraction alternate with darker, grainier, light gray intervals that contain echinoid spines as well as rare glauconite, pyrite, and unidentified black grains. Unit II (33–66 mbsf) is characterized by soft-sediment deformation interpreted as slumping. Two slumped intervals were identified, with the lower interval defining the boundary between Units II and III. Unit II consists of white to light gray, calcareous nannofossil ooze and calcareous nannofossil foraminifer ooze, as well as unlithified wackestones, packstones, floatstones, and rudstones. The light gray wackestones to rudstones contain a wide variety of coarse components, including various bryozoans (robust and delicate branching, arborescent, and fenestrate growth forms), bioclasts, sponge and tunicate spicules, and pellets. Pebble-sized lumps of calcareous nannofossil ooze, which are interpreted to be reworked clasts, occur in the packstones and floatstones. Unit III (66–152 mbsf) consists of calcareous nannofossil ooze and calcareous nannofossil foraminifer ooze. In the lower part of the unit, alternations between unlithified and lithified sediment are unlikely to be solely related to sediment compaction. The lower limit of alternating lithification corresponds to the base of Sequence 3 and thus may reflect condensed sedimentation related to this sequence boundary. The lower limit of Unit III is marked by a change from the dominantly pelagic sediments of Unit III to the partially lithified wackestones of Unit IV. Unit IV (152–214.3 mbsf) consists of unlithified to partially lithified wackestone/packstone, foraminifer chalk, and very minor packstone. The style of deposition is uniform throughout the unit, characterized by meter-scale alternations of light gray foraminifer chalk and light gray to gray wackestone/packstone. The unlithified to partially lithified wackestone/packstone contains similar components to the chalk, but it is richer in glauconite and dominated by bioclasts. Some of these layers have a sharp base and are normally graded, and they are interpreted to be turbidites. The lower boundary of Unit IV has been placed at the top of a white foraminifer chalk. Two main lithologies were recovered in Unit V (214.3–368.2 mbsf): (1) strongly bioturbated calcareous nannofossil chalk and (2) fragments of porcellanite and chert. The white chalk matrix is dominated by calcareous nannofossils with common sponge spicules as well as trace amounts of bioclasts and dolomite, whereas the coarse fraction consists of planktonic and benthic foraminifers. The gray and green porcellanite fragments are silicified chalk. Only 30 cm of core was recovered from Unit VI (368.2–397.1 mbsf), principally from the lowermost part of the unit. The sediments within this unit are coarse sand-sized, brown limonitic sandstones with quartz, limonite, glauconite, mica, and abundant skeletal grains, as well as minor planktonic foraminifers.

Calcareous nannofossils and planktonic foraminifers indicate that sediments recovered at Site 1134 range from Quaternary to middle Eocene in age. Two hiatuses are indicated: the first is within the Pliocene (nannofossil Zones NN18–NN13 missing at ~57 mbsf) and the second in the middle–upper Miocene (nannofossil Zones NN9–NN7 missing at ~114 mbsf). Planktonic foraminifers also indicate hiatuses at approximately the same depths. A third hiatus may be present in the Eocene section because nannofossil Zone NP17 was not recognized; however, poor core recovery makes confirmation of this hiatus difficult. Calcareous nannofossils are moderately well preserved above ~200 mbsf, with decreasing preservation below this level. Planktonic foraminifers are moderately well preserved throughout most of Hole 1134A, with preservation deteriorating only in the lowermost 30 m of the hole. Benthic foraminifers are generally rare compared to planktonic foraminifers, decreasing in abundance in the lower 130 m of Hole 1134A. Preservation of benthic foraminifers is comparable to that of the planktonic foraminifers. The five main assemblages of benthic foraminifers can be correlated with coeval assemblages at Site 1126 and indicate middle bathyal paleodepths. The benthic foraminifer record at Sites 1126 and 1134 appears excellent for evaluating changes in deep-water circulation in the Great Australian Bight during the Oligocene and Miocene.

Long-core measurements at Site 1134 indicate that the intensity of magnetization is extremely weak in the uppermost 100 mbsf, similar to that at Site 1126. However, discrete measurements revealed that a stable remanence is present, and the Brunhes/Matuyama boundary was identified in both holes. Magnetization intensity decreases to a minimum near 110 mbsf in a manner characteristic of the dissolution of fine magnetic particles. There is a marked increase in intensity to 120 mbsf, which coincides with the first appearance of chert at Site 1134. A brief magnetostratigraphy was determined within the Anomaly 5 sequence. Whole-core measurements and nonmagnetic coring experiments were conducted at this site, but the intensity of magnetization was so weak that further analysis is required from shore-based work.

Construction of a composite section for Site 1134 indicates that recovery of Holocene–middle Miocene sediments was complete to a depth of 151.7 mcd. The composite section was constructed primarily using 400-nm color reflectance, the 700:400 nm color reflectance ratio, and GRA bulk density data from Holes 1134A and 1134B. The mcd scale at Site 1134 is expanded by ~6% relative to the mbsf scale. The upper 35 m of sediment (lithostratigraphic Unit I) exhibits cyclic oscillations in color reflectance that are sufficiently distinctive to permit easy correlation between holes. Lithostratigraphic Unit II (34.7–68.9 mcd) contains two slumped intervals that yield excellent correlative horizons at their tops and bases. Lithostratigraphic Unit III (>68.9 mcd) is more difficult to correlate because of dissimilarities in the records from each hole, which may be a result of differential lithification and diagenesis.

Methane concentrations at Site 1134 were low, with maximum concentrations of 7.7 ppm and average concentrations less than 5 ppm. Calcium carbonate contents range from 58 to 94 wt%, averaging 80–92 wt%.

Site 1134 was characterized by a very steep gradient in pore-water salinity, reaching values of 97 by 65.90 mbsf. This salinity gradient is similar to that measured at Sites 1130 and 1126, and is consistent with the suggestion that the brine has a common level below the sea surface at all sites and is controlled by the level of the hydrostatic head during

sea-level lowstands. Because of the low rate of accumulation of organic material at Site 1134, oxidation rates of organic material and carbonate diagenesis are reduced compared to the more proximal (shallower water) sites. Significant geochemical reactions appear to take place only in the upper 40 mbsf at Site 1134. In this interval, there is a decrease in the concentration of metastable minerals (e.g., aragonite and HMC) and the appearance of small concentrations of dolomite. As a result, there is only a small increase in Sr^{2+} with depth—an increase that is quickly swamped by increases associated with greater salinity. The concentration of iron in interstitial waters from Site 1134 is higher than at shallower water, H_2S-dominated sites, reaching concentrations >60 mM.

Sediment physical properties measurements closely reflect lithologic variations and provide essential data for core-log correlation. These data were divided into four units based on variations in measured parameters. Physical properties Unit I (0–33 mbsf) is characterized by a sharp decrease in porosity (50%–30%) downhole, together with an increase in bulk density (1.7–2.0 g/cm^3) and *P*-wave velocity (1.6–1.8 km/s). This unit corresponds to the nannofossil ooze succession of lithostratigraphic Unit I. The top of PP Unit 2 is defined by an abrupt increase in bulk density and NGR and correlates with the transition from nannofossil ooze to unlithified bioclastic wackestone. Physical properties Unit 2 (33–66 mbsf) is typified by high variability in *P*-wave velocity, bulk density, and NGR that correlates with intervals of soft sediment deformation interpreted as slumps. Physical properties Unit 3 (66–145 mbsf) is characterized by a gradual decrease in bulk density and *P*-wave velocity, and a sharp decrease in NGR (10–2 cps) downhole. The lower part of the unit shows a marked increase in MS (negative values to ~10×10^{-6} SI units) and porosity. The base of PP Unit 3 is defined by an increase in NGR and a sharp decrease in MS. Physical properties Unit 4 (145–368 mbsf) shows highly variable *P*-wave velocity, bulk density, and porosity, which result from alternation of nannofossil oozes and wackestones/packstones in the upper part and alternation between chalk and chert in the lower part.

Three logging strings were successfully deployed in Hole 1134A. Overall, downhole measurement trends are similar to those at Site 1126C, but gamma-ray values at Site 1134 are markedly higher than at Site 1126C. The sedimentary succession at Site 1134 was divided into six logging units based on data trends that reflect lithologic alternations among the calcareous ooze, wackestone, grainstone, and thin chert interbed lithologies. Positive density and porosity separation and relatively high PEF values indicate the presence of dolomite toward the top of logging Unit 1. Narrow separation of density and porosity and relatively low PEF values indicate the presence of quartz in the carbonates of logging Unit 2. The presence of blackened grains in recovered cores coincides with higher gamma-ray values, indicating a possible phosphatic and/or glauconitic component. Downhole logs also identify an interval of unusually low potassium concentrations in logging Unit 3, the significance of which is still to be established. Density, PEF, caliper, and resistivity were the only logs acquired within the sandstones at the base of the succession (logging Unit 6). High density and high PEF peaks are consistent with the small amount of limonitic sandstone recovered from this horizon, which may correspond to logging Unit 8 at Hole 1126C. Seven check-shot stations were recorded, with individual stations situated near the estimated depths of significant reflectors.

Correlation of Site 1134 data with the regional seismic grid permits further refinement of the Eucla Basin Cenozoic seismic stratigraphy

(Feary and James, 1998, reprinted as Chap. 2). Data from Site 1134 confirm the Pleistocene–upper Pliocene age of the seismic Sequence 2 nannofossil ooze and nannofossil foraminifer ooze, the middle–late Miocene age of the nannofossil ooze and nannofossil foraminifer ooze of Sequence 3, and the early Miocene age of the alternating foraminifer chalk and unlithified to partially lithified wackestone/packstone lithologies of Sequence 4. It also establishes that the uppermost Lobe 3 component of seismic Sequence 6A is of late Oligocene age, consisting of partially silicified, bioturbated, calcareous nannofossil chalk. The middle Lobe 2 part of Sequence 6A has a similar lithology, and spans the upper Eocene–lower Oligocene. The middle Eocene limonitic sandstone poorly recovered at the base of Site 1134 is assigned to seismic Sequence 7.

REFERENCES

Bein, J., and Taylor, M.L., 1981. The Eyre Sub-basin: recent exploration results. *APEA J.,* 21:91–98.

Bone, Y., James, N.P., and Kyser, T.K., 1992. Syn-sedimentary detrital dolomite in Quaternary cool-water carbonate sediments, Lacepede Shelf, south Australia. *Geology,* 20:109–112.

Boreen, T.D., and James, N.P., 1993. Holocene sediment dynamics on a cool-water carbonate shelf, southeastern Australia. *J. Sediment. Petrol.,* 63:574–588.

Davies, H.L., Clarke, J.L.A., Stagg, H.M.J., Shafik, S., McGowran, B., and Willcox, J.B., 1989. Maastrichtian and younger sediments from the Great Australian Bight. *Bur. Miner. Resour. Aust. Rec.,* 288.

Eberli, G.P., Swart, P.K., Malone, M.J., et al., 1997. *Proc. ODP, Init. Repts.,* 166: College Station, TX (Ocean Drilling Program).

Feary, D.A., 1995. Proposal for an ODP site survey cruise by the R/V Rig Seismic in the western Great Australian Bight. *Aust. Geol. Surv. Org.,* 67.

Feary, D.A., and James, N.P., 1995. Cenozoic biogenic mounds and buried Miocene (?) barrier reef on a predominantly cool-water carbonate continental margin, Eucla Basin, western Great Australian Bight. *Geology,* 23:427–430.

————, 1998. Seismic stratigraphy and geological evolution of the Cenozoic, cool-water, Eucla Platform, Great Australian Bight. *AAPG Bull.,* 82:792–816.

Feary, D.A., James, N.P., and McGowran, B., 1994. Cenozoic cool-water carbonates of the Great Australian Bight: reading the record of Southern Ocean evolution, sea level, paleoclimate, and biogenic production. *Aust. Geol. Surv. Org.,* 62.

Feary, D.A., James, N.P., McGowran, B., and Smart, P.L., 1995. Cenozoic cool-water carbonates of the Great Australian Bight: reading the record of Southern Ocean evolution, sealevel, paleoclimate, and biogenic production. *Aust. Geol. Surv. Org.,* 78.

Haq, B.U., Hardenbol, J., and Vail, P.R., 1987. Chronology of fluctuating sea levels since the Triassic. *Science,* 235:1156–1167.

Hegarty, K.A., Weissel, J.K., and Mutter, J.C., 1988. Subsidence history of Australia's southern margin: constraints on basin models. *AAPG Bull.,* 72:615–633.

James, J.M., 1992. Corrosion par melange des eaux dans les grottes de la plaine de Nullarbor, Australie. *In* Salomon, J.N., and Maire, R. (Eds.), *Karst et Evolutions Climatiques: Hommage a Jean Nicod:* Talence, France (Univ. Bordeaux), 333–348.

James, J.M., Rogers, P., and Spate, A.P., 1989. Genesis of the caves of the Nullarbor Plain, Australia. *Proc. 10th Int. Congr. Speleol.,* 263–265.

James, N.P., and Bone, Y., 1991. Origin of a cool-water, Oligo-Miocene deep shelf limestone, Eucla Platform, southern Australia. *Sedimentology,* 38:323–342.

James, N.P., Bone, Y., and Kyser, T.K., 1993. Shallow burial dolomitization of Cenozoic cool-water calcitic deep shelf limestones, southern Australia. *J. Sediment. Petrol.,* 63:528–538.

James, N.P., and Kendall, A.C., 1992. Introduction to carbonate and evaporite facies models. *In* Walker, R.G., and James, N.P. (Eds.), *Facies Models: Response to Sea Level Change:* St. Johns, Newfoundland (Geol. Assoc. Can.), 265–276.

James, N.P., and von der Borch, C.C., 1991. Carbonate shelf edge off southern Australia: a prograding open-platform margin. *Geology,* 19:1005–1008.

Kendall, C.G.St.C., and Schlager, W., 1981. Carbonates and relative changes in sea level. *In* Cita, M.B., and Ryan, W.B.F. (Eds.), *Carbonate Platforms of the Passive-type Continental Margins, Present and Past.* Mar. Geol., 44:181–212.

Kennett, J.P., 1982. *Marine Geology:* Englewood Cliffs, NJ (Prentice-Hall).

Kennett, J.P., and Barker, P.F., 1990. Latest Cretaceous to Cenozoic climate and oceanographic developments in the Weddell Sea, Antarctica: an ocean-drilling perspective. *In* Barker, P.F., Kennett, J.P., et al., *Proc. ODP, Sci. Results,* 113: College Station, TX (Ocean Drilling Program), 937–960.

Kennett, J.P., and Barron, J.A., 1992. Introduction. *In* Kennett, J.P., and Warnke, D.A. (Eds.), *The Antarctic Paleoenvironment: A Perspective on Global Change*. Am. Geophys. Union, 56:1–6.

Marshall, J.F., 1986. Regional distribution of submarine cements within an epicontinental reef system: central Great Barrier Reef, Australia. *In* Schroeder, J.H., and Purser, B.H. (Eds.), *Reef Diagenesis:* Berlin (Springer-Verlag), 8–26.

McKenzie, J.A., Isern, A., Elderfield, H., Williams, A., and Swart, P., 1993. Strontium isotope dating of paleoceanographic, lithologic, and dolomitization events on the northeastern Australian margin, Leg 133. *In* McKenzie, J.A., Davies, P.J., Palmer-Julson, A., et al., *Proc. ODP, Sci. Results,* 133: College Station, TX (Ocean Drilling Program), 489–498.

Miller, K.G., Fairbanks, R.G., and Mountain, G.S., 1987. Tertiary oxygen isotope synthesis, sea-level history, and continental margin erosion. *Paleoceanography,* 2:1–19.

Nelson, C.S., 1988. An introductory perspective on non-tropical shelf carbonates. *Sediment. Geol.,* 60:3–12.

Reeckmann, S.A., 1988. Diagenetic alterations in temperate shelf carbonates from southeastern Australia. *In* Nelson, C.S., (Ed.), *Non-tropical Shelf Carbonates: Modern and Ancient.* Sediment. Geol., 60:209–219.

Rockford, D.J., 1986. Seasonal changes in the distribution of Leeuwin Current waters off southern Australia. *Aust. J. Mar. Freshwater Res.,* 37:1–10.

Sarg, J.F., 1988. Carbonate sequence stratigraphy. *In* Wilgus, C.K., Hastings, B.S., Kendall, C.G.St.C., Posamentier, H., Ross, C.A., and Van Wagoner, J. (Eds.), *Sea-Level Changes: An Integrated Approach.* Spec. Publ.—Soc. Econ. Paleontol. Mineral., 42:155–181.

Simms, M., 1984. Dolomitization by groundwater-flow systems in carbonate platforms. *Trans. Gulf Coast Assoc. Geol. Soc.,* 34:411–420.

Stagg, H.M.J., Cockshell, C.D., Willcox, J.B., Hill, A.J., Needham, D.J.L., Thomas, B., O'Brien, G.W., and Hough, L.P., 1990. *Basins of the Great Australian Bight region: geology and petroleum potential*. Cont. Marg. Progr., Bur. Miner. Resour. Aust., Fol., 5.

Vahrenkamp, V.C., Swart, P.K., and Ruiz, J., 1991. Episodic dolomitization of late Cenozoic carbonates in the Bahamas: evidence from strontium isotopes. *J. Sediment. Petrol.,* 61:1002–1014.

Willcox, J.B., Stagg, H.M.J., Davies, H.L., et al., 1988. Rig Seismic research cruises 10 & 11: geology of the Central Great Australian Bight region. *Rep.—Bur. Mineral Resour. Geol. Geophys. (Aust.),* 286.

Figure F1. Location of the Leg 182 drill sites in the western Great Australian Bight.

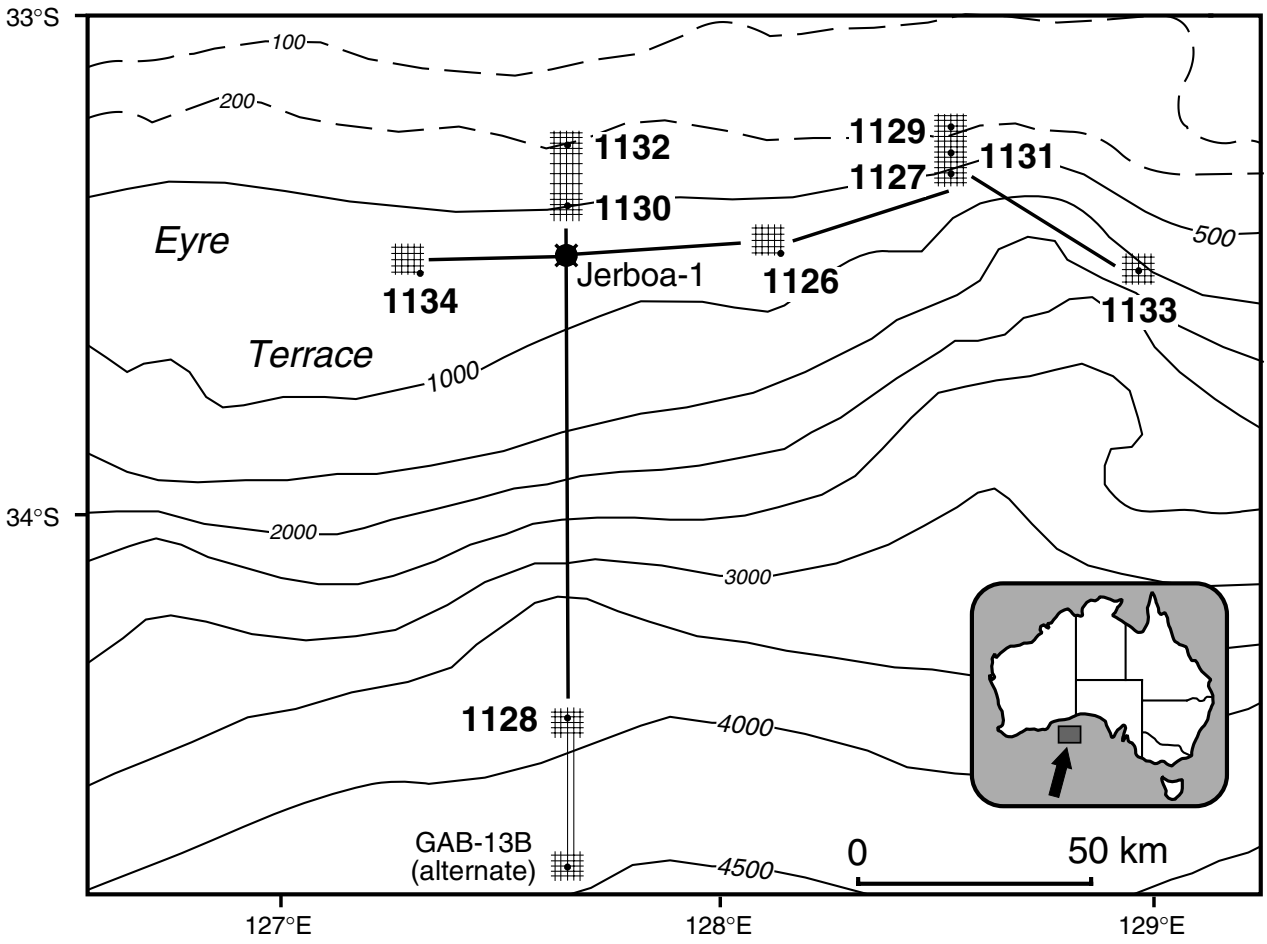

Figure F2. Schematic north-south diagram from the Nullarbor Plain to the upper continental slope across the Eyre Terrace (along longitude 128°E), showing the distribution and internal relationships of seven Cenozoic sequences (shown in blue in the top diagram) defined from seismic data, overlying Mesozoic synrift siliciclastic sequences (green), and Precambrian crystalline basement (brown) (after Feary and James, 1998, reprinted as Chap. 2). Vertical scales are approximate.

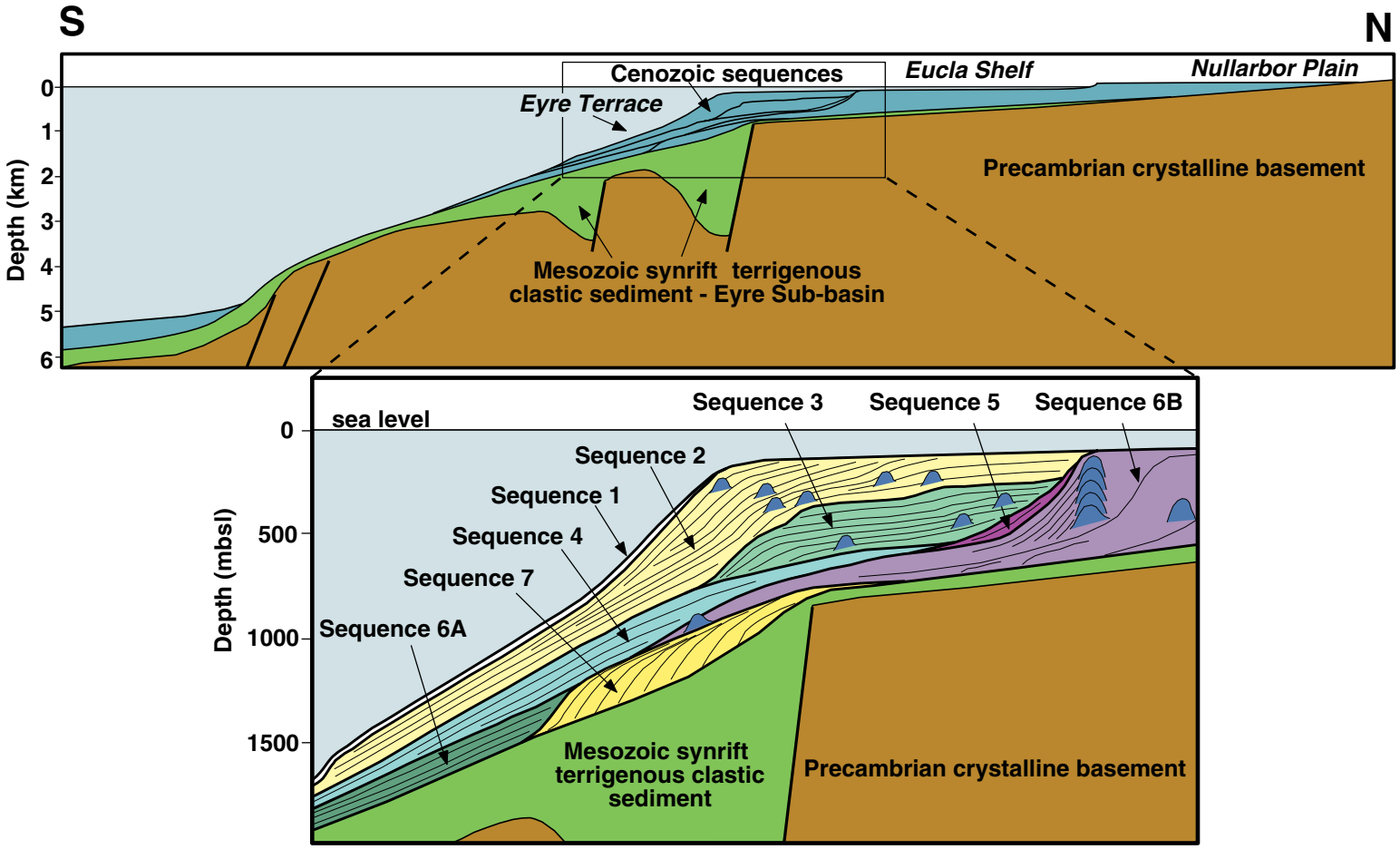

Figure F3. Lithostratigraphic summary of the western transect. Inset is a schematic north-south diagram showing the distribution of the western transect sites.

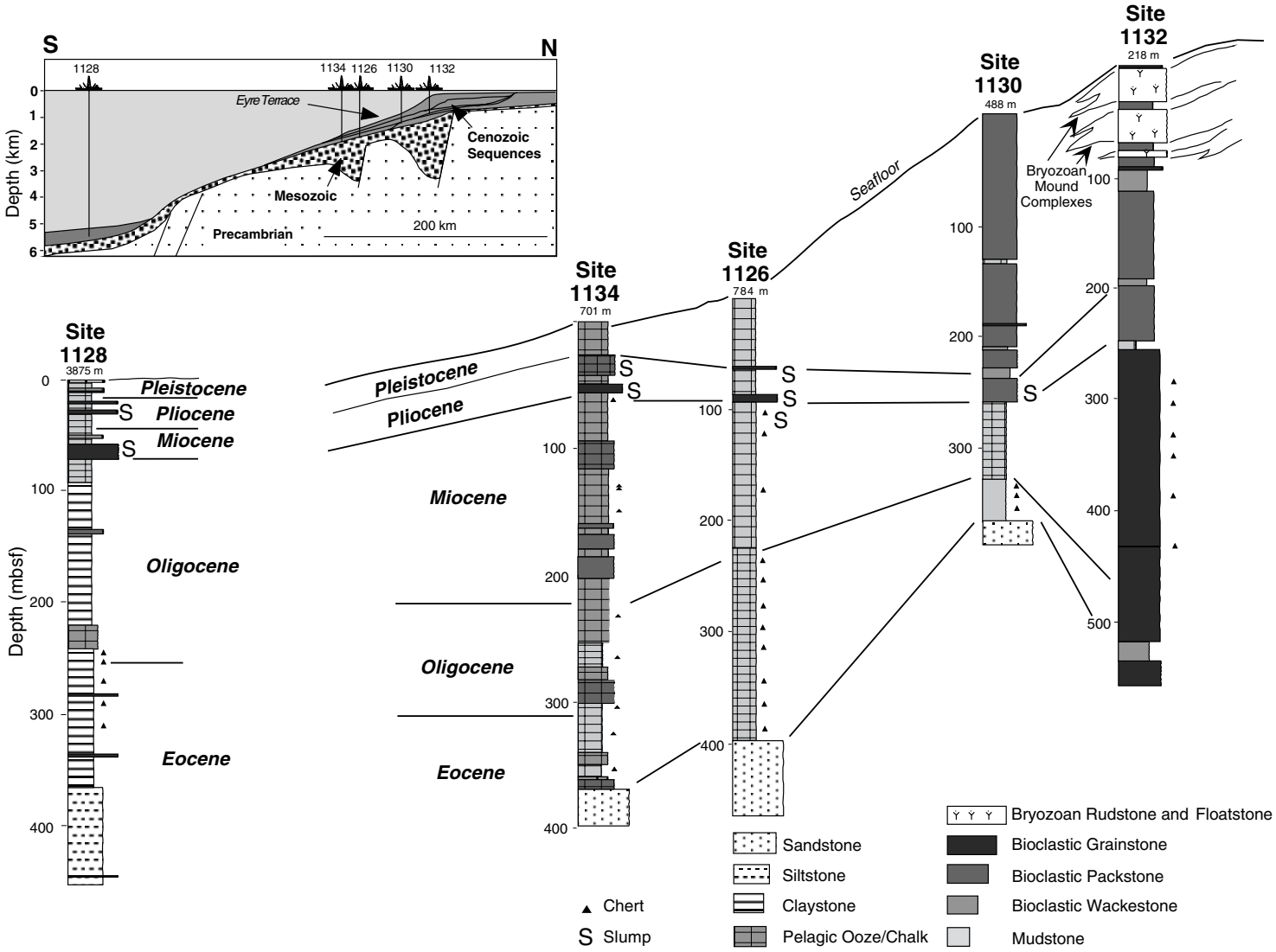

Figure F4. Lithostratigraphic summary of the eastern transect. Inset is an interpreted seismic line showing the distribution of the eastern transect sites.

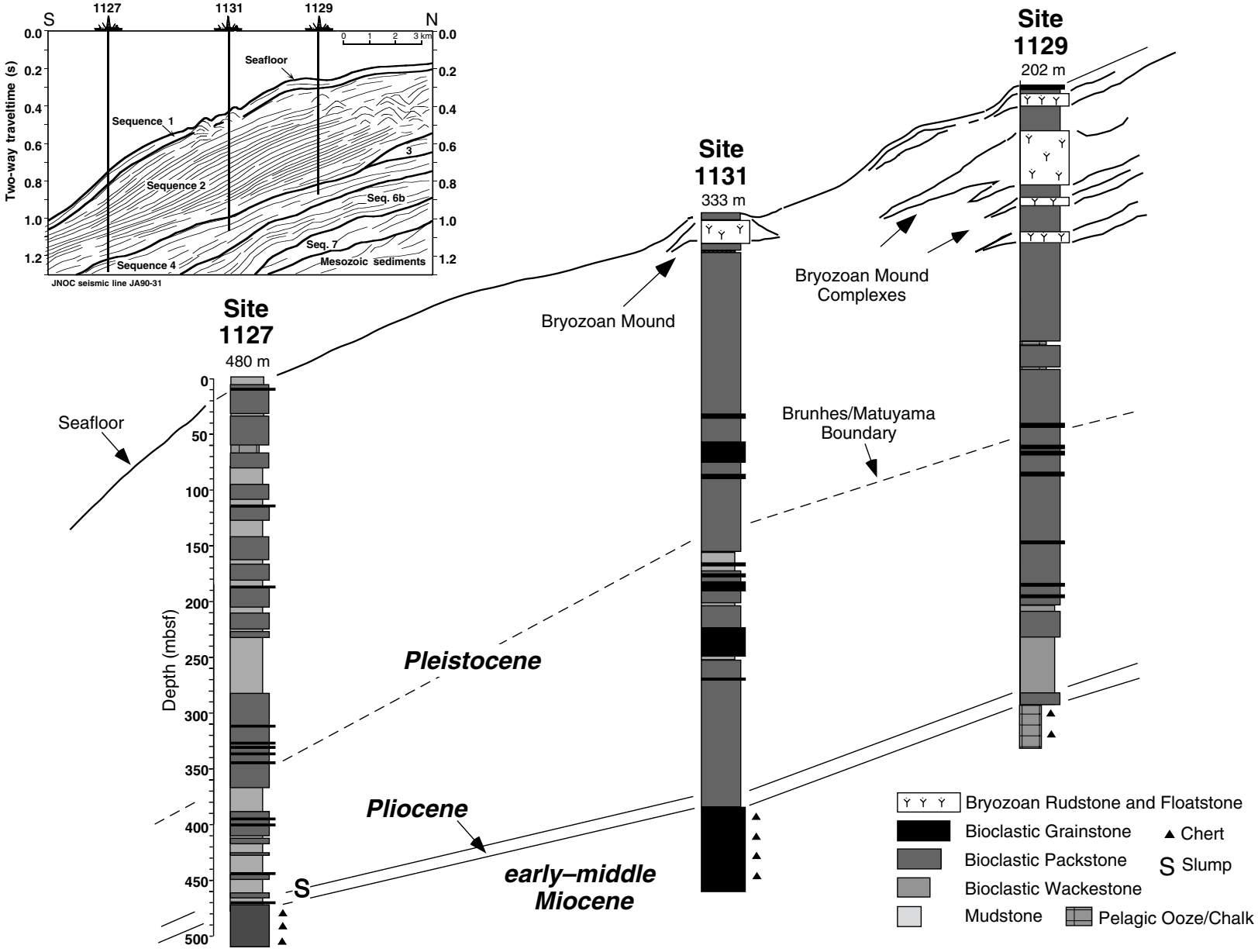

Figure F5. Major biostratigraphic units, unconformities, and paleobathymetric units recorded at Leg 182 sites.

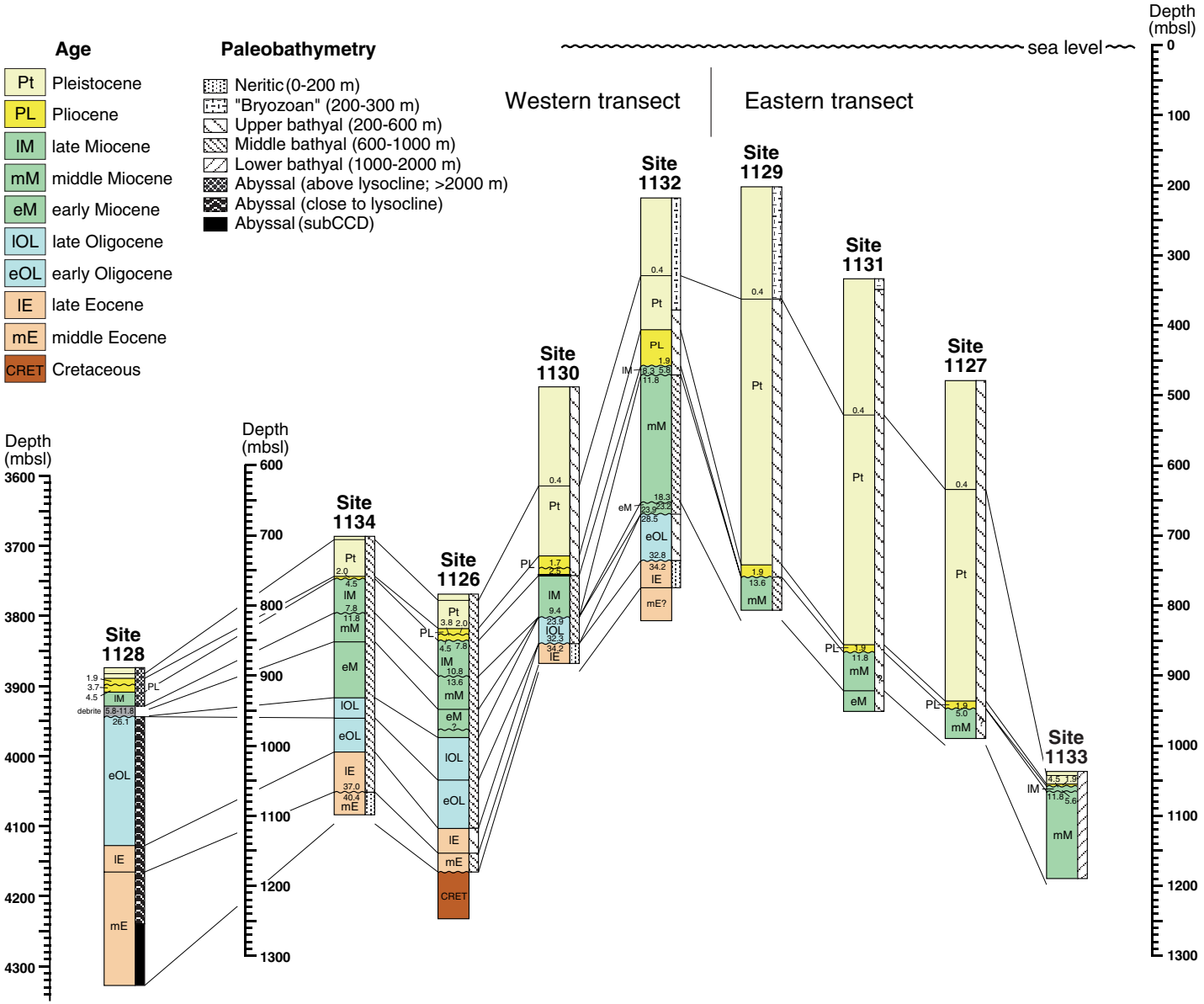

Figure F6. Age-depth plots of biostratigraphic datum levels, showing major hiatuses and estimated sedimentation rates. Datum controls are weaker in stratigraphically older sections, partly as a result of poor preservation and partly as a result of the temperate nannofossil and foraminiferal assemblages that contain few age-diagnostic species.

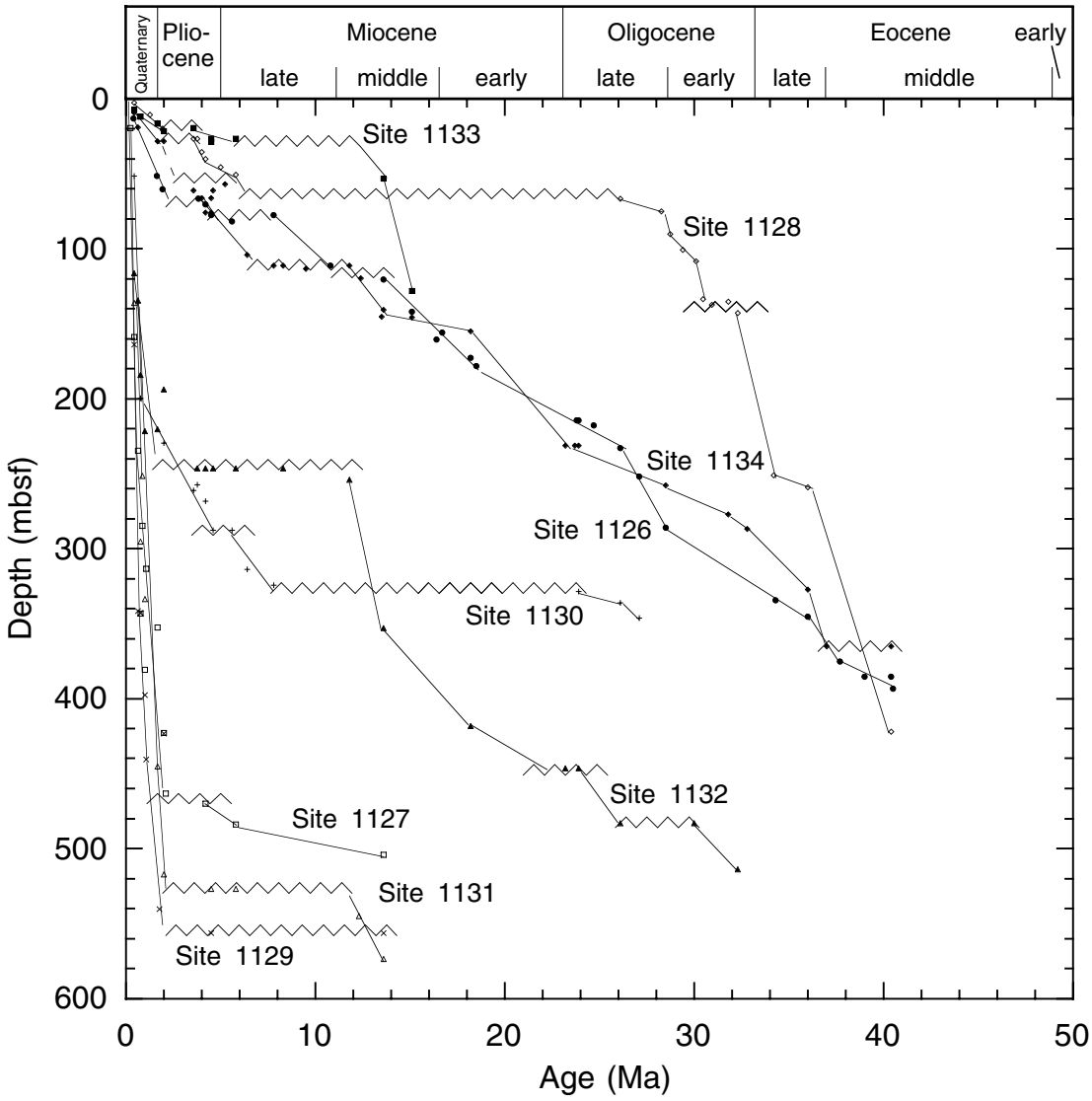

Figure F7. Summary of paleomagnetic data (inclination) and interpreted magnetostratigraphy for sites on the (A) eastern shelf-slope transect of Leg 182. Cross symbols are long-core measurements at 5–10 cm intervals, whereas discrete samples and lithified core fragments are shown as open symbols. (Continued on next page.)

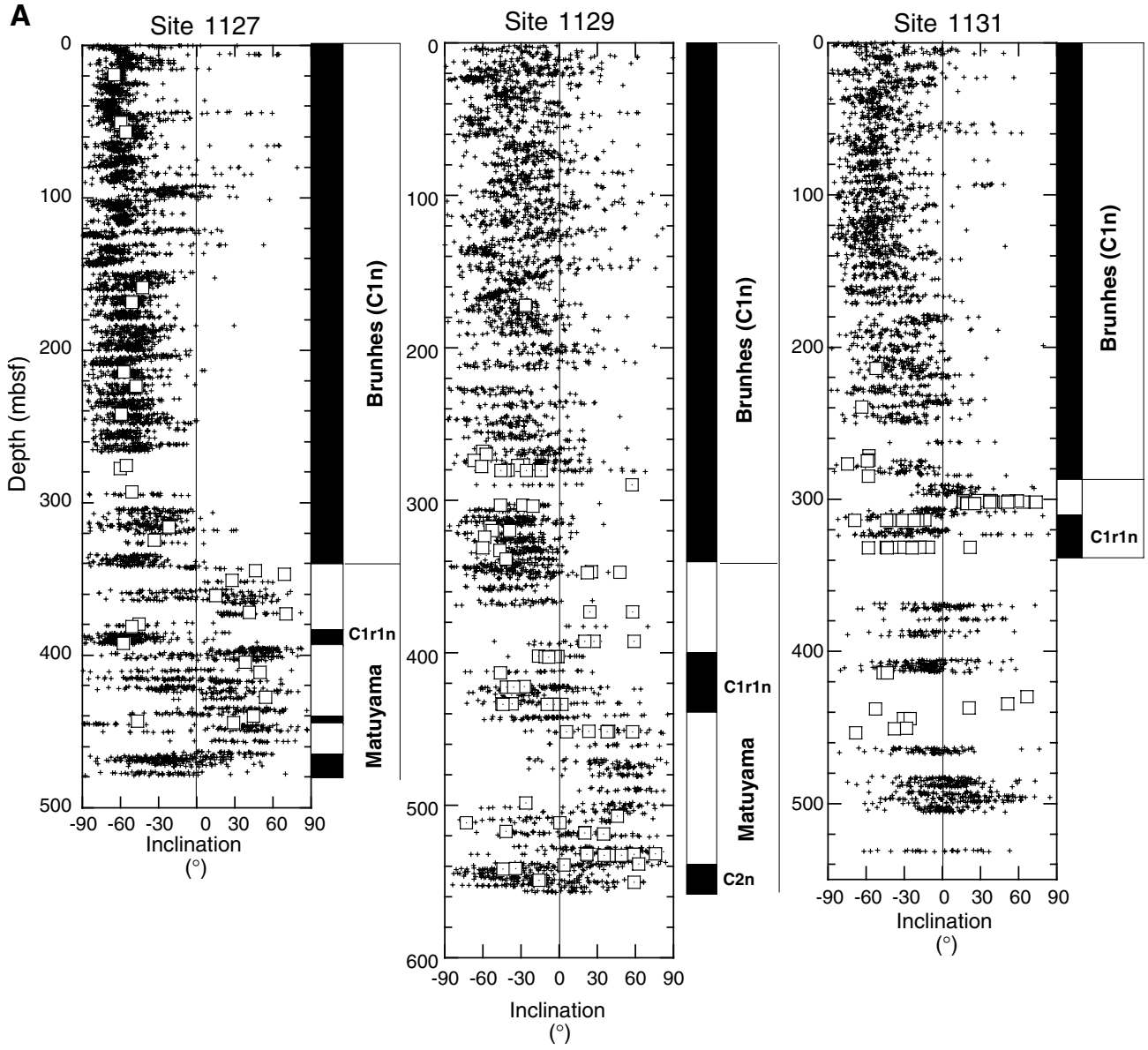

Figure F7 (continued). Summary of paleomagnetic data (inclination) and interpreted magnetostratigraphy for sites on the (**B**) western shelf-slope transect of Leg 182. Cross symbols are long-core measurements at 5–10 cm intervals, whereas discrete samples and lithified core fragments are shown as open symbols. The interpreted magnetostratigraphy is the same for Holes 1130A and 1130B.

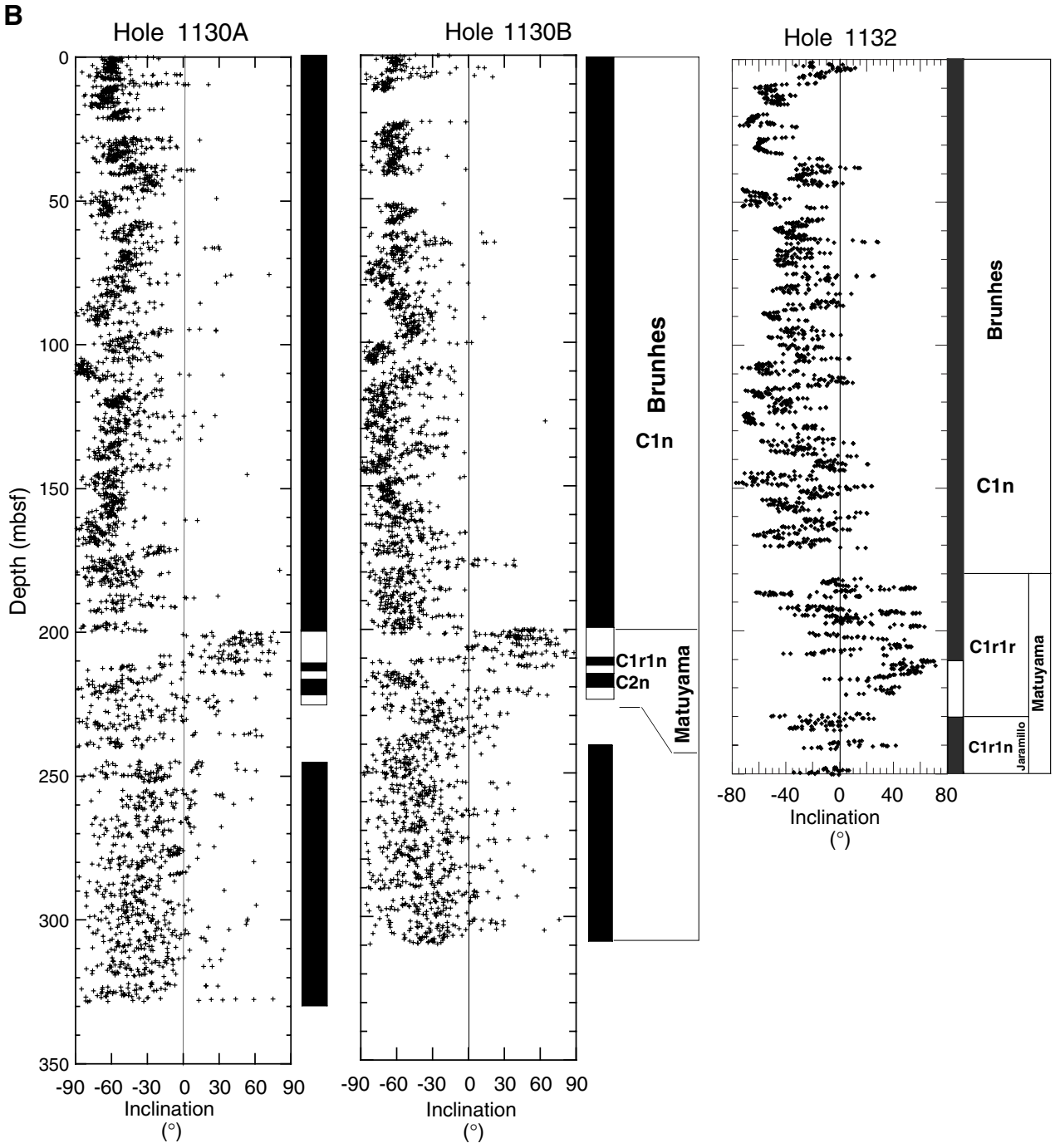

Figure F8. Contour plot of Cl^- concentration at Sites 1127, 1131, and 1129, displayed overlying the interpretation of a seismic line joining the three sites. Note that the lines of equal Cl^- concentration crosscut the seismic sequences and appear to originate from a subhorizontal brine. Cl^- concentrations are given in millimoles per liter (mM). Normal seawater concentration is 559 mM.

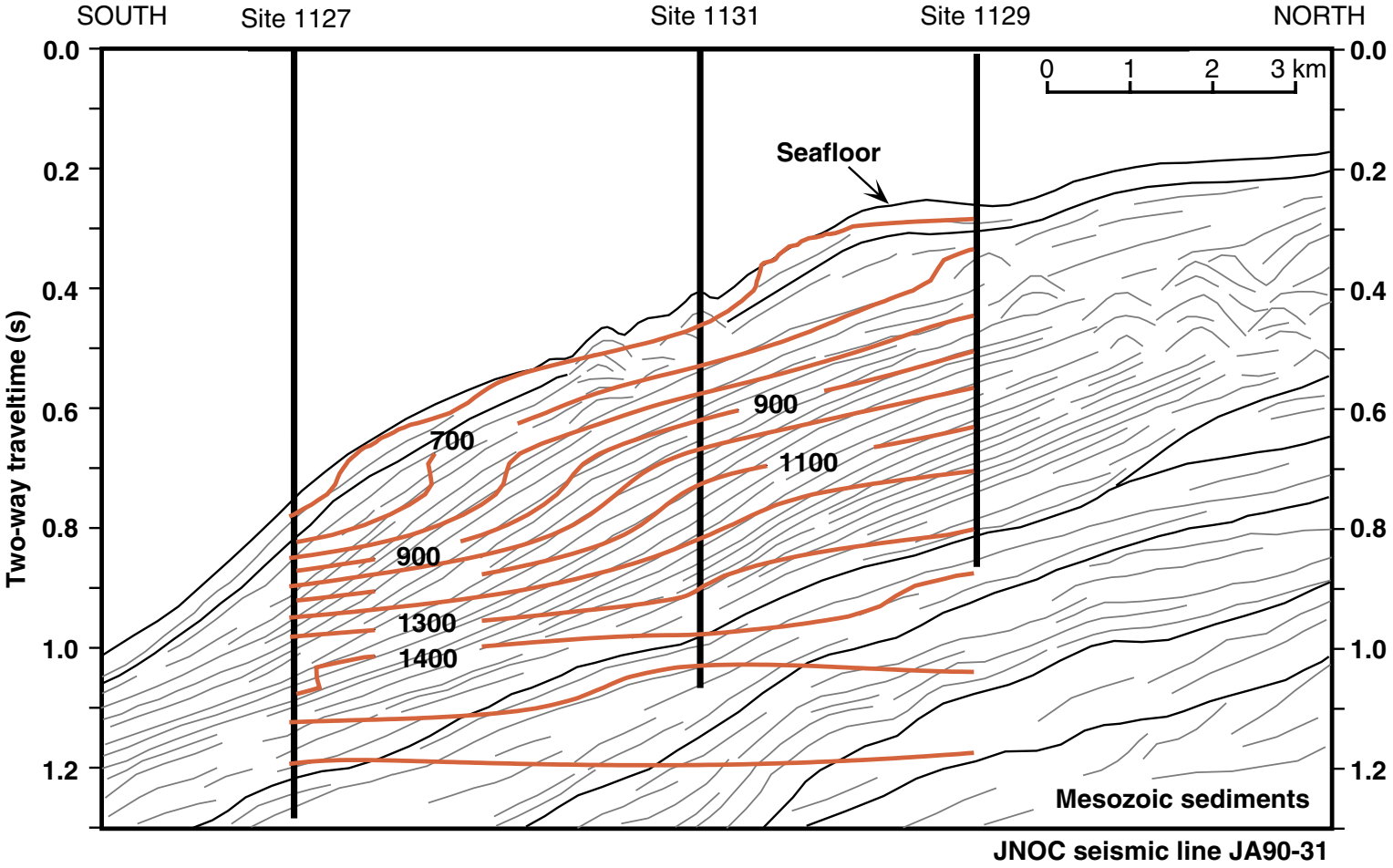

Figure F9. Concentration of methane (circles), ethane (triangles), and propane (diamonds) in headspace samples from Site 1129. Note the maximum in concentration of all three gaseous species occurs between 200 and 500 mbsf. This is particularly significant for the higher weight alkanes and suggests that they are not migrating from deeper in the section.

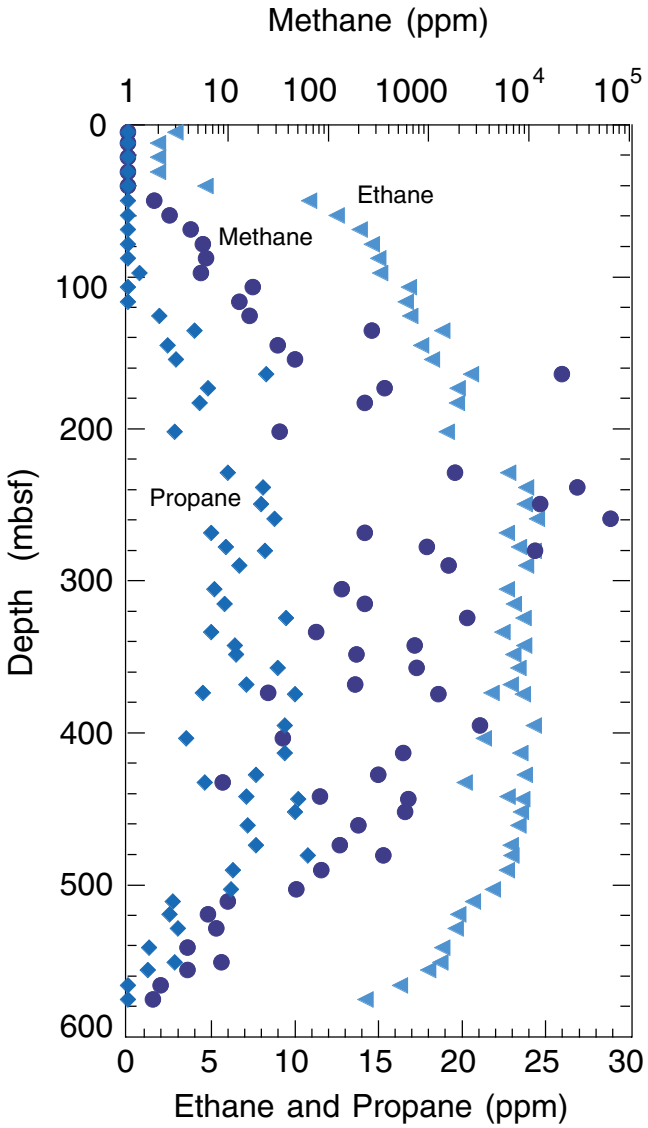

Figure F10. Concentration of dolomite at Sites 1127, 1131, and 1129. The highest sustained concentrations (10–15 wt%) occur at Sites 1129 and 1131, although samples with values as high as 35 wt% were measured at Site 1127. The dolomitization is principally associated with the Quaternary sediments.

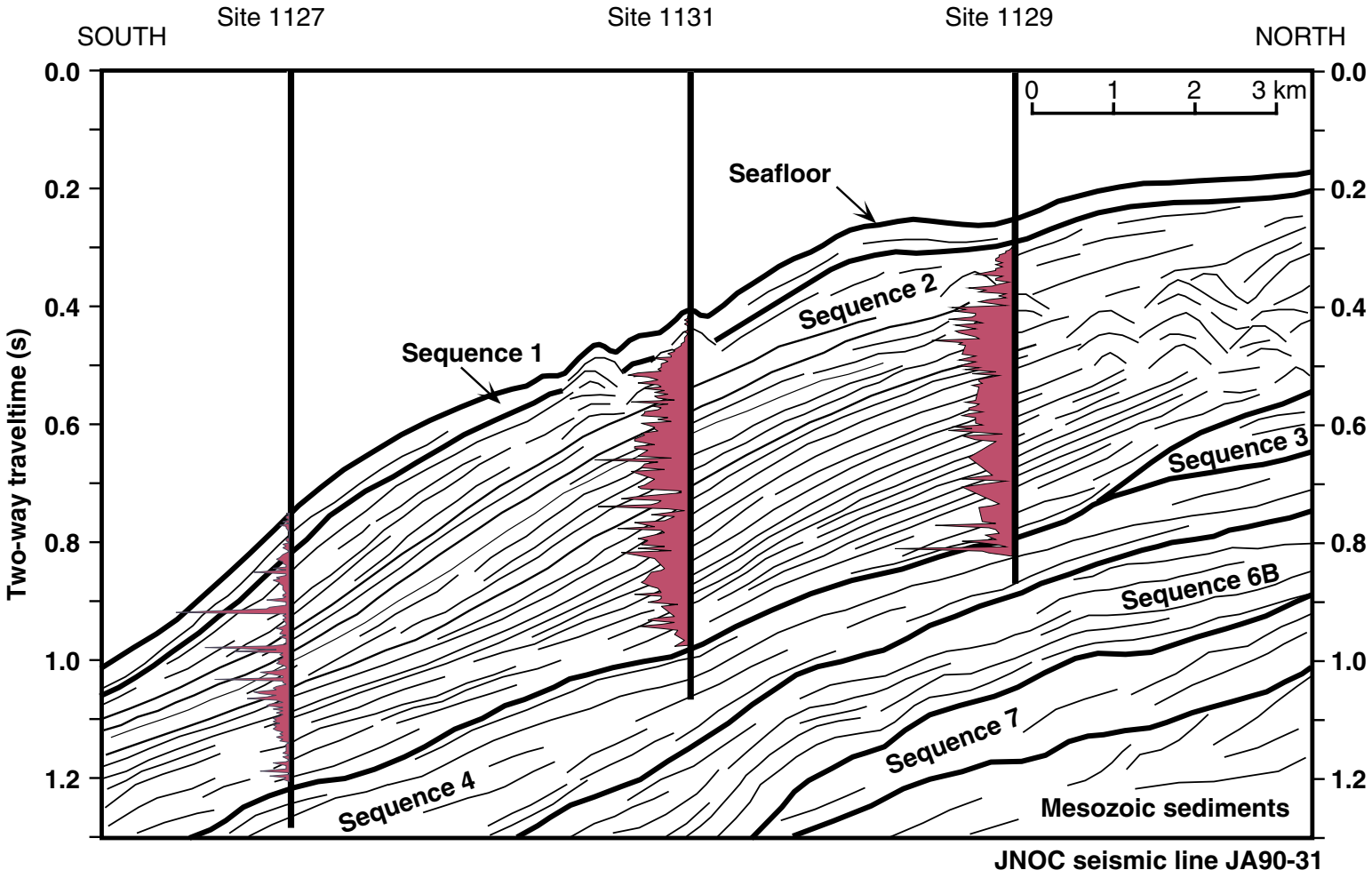

Figure F11. Japan National Oil Corporation (JNOC) seismic line JA90-31 for the eastern drilling transect, overlain with spectral gamma radiation (right curve at each site), bulk density (left curve at Sites 1131 and 1129), and porosity (left curve at Site 1127) from the downhole logs. Because of high hydrogen sulfide in the drill hole at Site 1127, the nuclear source of the hostile environment lithodensity sonde was not used. Thus, there are no bulk density estimates for this site. All data were converted to two-way traveltime using a linear interpolation of traveltime from the seafloor to the bottom of the drilled interval.

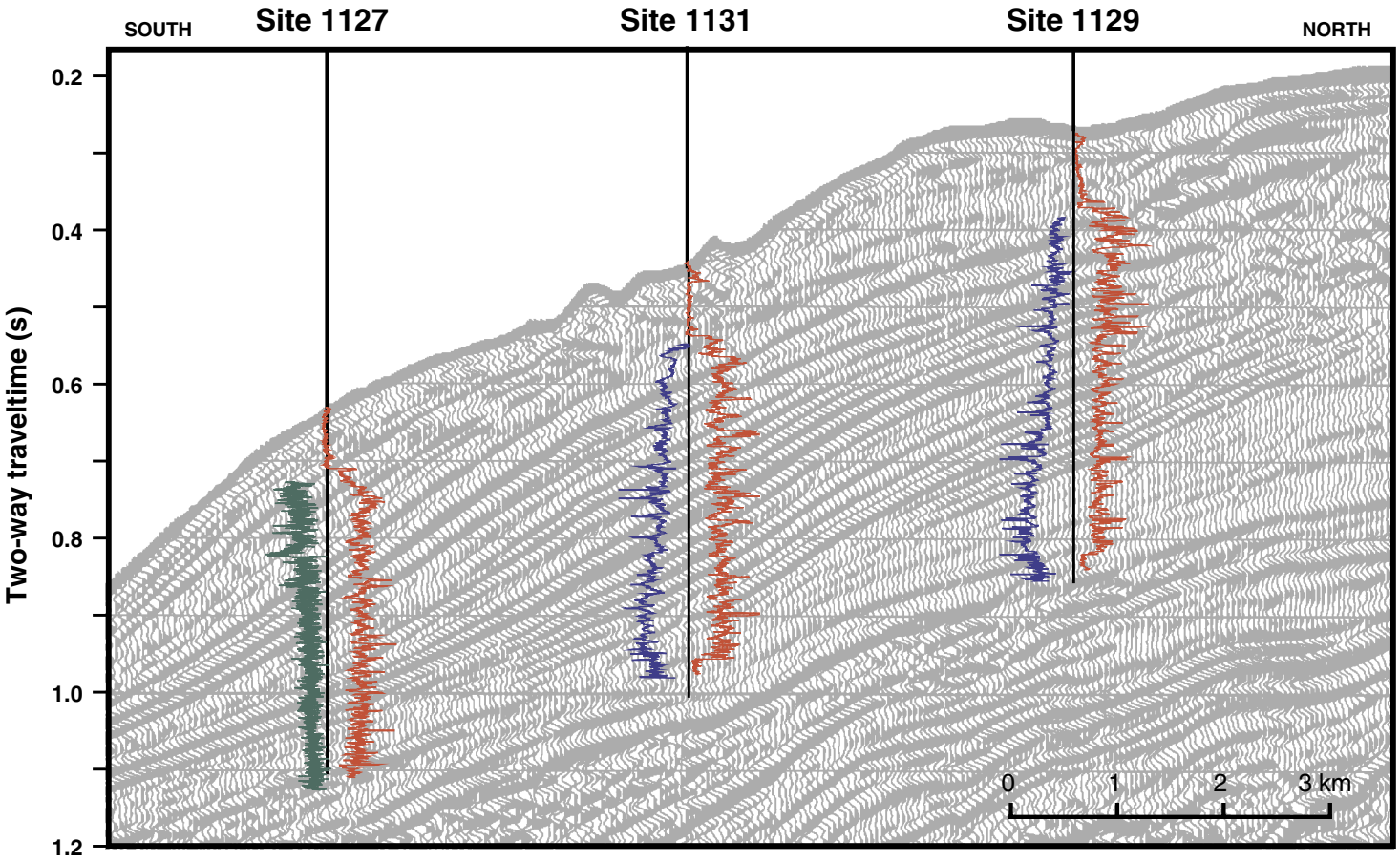

Table T1. Summary of Quaternary magnetostratigraphy.

Polarity events and age	Chron boundaries	Hole 1127B depth (mbsf)	Hole 1128B depth (mbsf)	Holes 1129C, 1129D depth (mbsf)	Hole 1130B depth (mbsf)	Hole 1131A depth (mbsf)	Hole 1132B depth (mbsf)	Hole 1133B depth (mbsf)	Hole 1134A depth (mbsf)
Brunhes/ Matuyama	C1n/C1r1r	343.4	14	340	200	280–300	170-181	12	32
0.78 Ma		1127B-37X-4	1128B-2H-4	1129C-37X-3	1130B-22X-4	1131A-33X-3, 4	1132B-19X-21X	1133B-3H-1	1134A-4H-6
Termination Jaramillo	C1r1r/C1r1n	380.7	20	392-402	210	308	222–229		37
0.99 Ma		1127B-41X-4	1128B-3H-2	1129D-5R-6R	1130B-23X-4	1131A-34X-3	1132B-25X, 26X		1134A-5H-4
Onset Jaramillo	C1r1n/C1r2r1r	393-395	22	435-445	212				41
1.07 Ma		1127B-42X-5, 6	1128B-3H-4	1129D-9R-10R	1130B-23X-6				1134A-5H-6
Termination Olduvai	C1r2r2r/C2n		28	540	215				
1.77 Ma			1128B-4H-1	1129D-20R-3	1130B-24X-1				
Onset of Olduvai	C2n/C2r		32		220				
1.95 Ma			1128B-4H-4		1130B-24X-5				
Termination of Gauss	C2r/C2An		40						
2.5 Ma			1128B-5H-3						

Note: Section numbers in site depth columns identify location of chron boundaries for each site.

Table T2. Summary of operations.

Hole	Latitude	Longitude	Water depth (mbsf)	Number of cores	Length cored (m)	Length recovered (m)	Recovery (%)	Interval drilled (m)	Total penetration (mbsf)	Time on site (days)
1126A	33°30.5615′S	128°03.9957′E	784.8	1	9.5	9.69	102.0%	0.0	9.5	0.3
1126B	33°30.5613′S	128°03.9922′E	783.7	30	253.5	162.55	64.1%	9.8	263.3	1.3
1126C	33°30.5638′S	128°04.0101′E	783.8	17	154.0	138.52	89.9%	0.0	154.0	0.7
1126D	33°30.5613′S	128°03.9844′E	783.8	33	313.3	40.47	12.9%	150.0	463.3	2.4
			Site 1126 totals:	81	730.3	351.23	48.1%	159.8	890.1	4.7
1127A	33°21.4457′S	128°28.8780′E	478.7	1	9.5	9.68	101.9%	0.0	9.5	0.1
1127B	33°21.4504′S	128°28.8765′E	479.3	55	510.7	440.36	86.2%	0.0	510.7	3.2
			Site 1127 totals:	56	520.2	450.04	86.5%	0.0	520.2	3.4
1128A	34°23.4686′S	127°35.4419′E	3875.8	1	9.5	9.31	98.0%	0.0	9.5	0.4
1128B	34°23.4706′S	127°35.4455′E	3874.6	30	280.7	231.57	82.5%	0.0	280.7	1.8
1128C	34°23.4633′S	127°35.4619′E	3874.3	26	240.1	232.84	97.0%	0.0	240.1	1.5
1128D	34°23.4563′S	127°35.4554′E	3874.3	23	221.4	79.08	35.7%	231.2	452.6	3.9
			Site 1128 totals:	80	751.7	552.80	73.5%	231.2	982.9	7.6
1129A	33°17.3857′S	128°28.8718′E	202.9	2	13.8	13.27	96.2%	9.5	23.3	0.3
1129B	33°17.3783′S	128°28.8606′E	202.3	2	19.0	10.24	53.9%	22.0	41.0	0.3
1129C	33°17.7942′S	128°28.8785′E	202.5	48	451.6	322.89	71.5%	0.0	451.6	0.8
1129D	33°17.7887′S	128°28.8675′E	202.1	26	250.6	76.72	30.6%	353.6	604.2	2.2
			Site 1129 totals:	78	735.0	423.12	57.6%	385.1	1120.1	3.6
1130A	33°25.2113′S	127°36.1398′E	486.7	41	380.4	312.47	82.1%	0.0	380.4	1.9
1130B	33°25.2091′S	127°36.1249′E	488.2	33	310.4	300.80	96.9%	0.0	310.4	0.8
1130C	33°25.1988′S	127°36.1248′E	488.1	10	96.0	23.30	24.3%	299.2	395.2	1.7
			Site 1130 totals:	84	786.8	636.57	80.9%	299.2	1086.0	4.4
1131A	33°19.5655′S	128°28.8721′E	333.6	66	616.9	371.69	60.3%	0.0	616.9	3.2
1131B	33°19.5541′S	128°28.8528′E	331.4	12	105.8	95.14	89.9%	0.0	105.8	0.6
			Site 1131 totals:	78	722.7	466.83	64.6%	0.0	722.7	3.8
1132A	33°18.9569′S	127°36.1304′E	218.0	1	9.3	9.23	99.2%	0.0	9.3	0.1
1132B	33°18.9713′S	127°36.1322′E	218.5	32	284.6	217.35	76.4%	0.0	284.6	1.1
1132C	33°18.9624′S	127°36.1235′E	218.5	39	366.2	22.42	6.1%	237.0	603.2	2.6
			Site 1132 totals:	72	660.1	249.00	37.7%	237.0	897.1	3.8
1133A	33°32.3694′S	128°54.3063′E	1037.2	1	9.5	9.78	102.9%	0.0	9.5	0.2
1133B	33°32.3783′S	128°54.3173′E	1037.2	19	152.1	48.59	31.9%	0.0	152.1	0.8
1133C	33°32.3887′S	128°54.32098′E	1036.8	6	53.3	37.26	69.9%	0.0	53.3	0.6
			Site 1133 totals:	26	214.9	95.63	44.5%	0.0	214.9	1.6
1134A	33°31.7244′S	127°15.8400′E	701.0	43	397.1	195.54	49.2%	0.0	397.1	2.4
1134B	33°31.7388′S	127°15.8377′E	699.9	25	234.8	158.76	67.6%	0.0	234.8	0.9
			Site 1134 totals:	68	631.9	354.30	56.1%	0.0	631.9	3.3
			Leg 182 totals:	623	5753.6	3579.52	62.2%	1312.3	7065.9	36.3